Volume 5, Issue 9 – July – December – 2019

ECORFAN

Journal-Democratic Republic of Congo

ISSN-On line 2414-4924

10th ANNIVERSARY ECORFAN Special Edition

ECORFAN Journal - Democratic Republic of Congo, Volume 5, Issue 9, July-December 2019, is a journal edited semestral by ECORFAN. 6593 Kinshasa 31Rép.DémocratiqueduCongo.WEB:www.ecorfan.org/DemocraticRepublicofCongo/,journal@ec orfan.org. Editor in Chief: ILUNGA-MBUYAMBA, Elisée. MsC. ISSN On line: 2414-4924. Responsible for the latest update of this number ECORFAN Computer Unit. ESCAMILLA-BOUCHÁN, Imelda. PhD, LUNA-SOTO, Vladimir. PhD, 6593 Kinshasa 31Rép. Démocratique du Congo, last updated December 31, 2019.

ECORFAN-Democratic Republic of Congo

Definition of Journal

Scientific Objectives

Support the international scientific community in its written production Science, Technology and Innovation in the Field of Physical Sciences Mathematics and Earth sciences, in Subdisciplines of image and signal processing, control-digital system-artificial, intelligence-fuzzy, logic-mathematical, modeling-computational, mathematics-computer, science.

ECORFAN-Mexico SC is a Scientific and Technological Company in contribution to the Human Resource training focused on the continuity in the critical analysis of International Research and is attached to CONACYT-RENIECYT number 1702902, its commitment is to disseminate research and contributions of the International Scientific Community, academic institutions, agencies and entities of the public and private sectors and contribute to the linking of researchers who carry out scientific activities, technological developments and training of specialized human resources with governments, companies and social organizations.

Encourage the interlocution of the International Scientific Community with other Study Centers in Mexico and abroad and promote a wide incorporation of academics, specialists and researchers to the publication in Science Structures of Autonomous Universities - State Public Universities - Federal IES - Polytechnic Universities - Technological Universities - Federal Technological Institutes - Normal Schools - Decentralized Technological Institutes - Intercultural Universities - S & T Councils - CONACYT Research Centers.

Scope, Coverage and Audience

ECORFAN-Democratic Republic of Congo is a Journal edited by ECORFAN-Mexico S.C in its Holding with repository in Democratic Republic of Congo, is a scientific publication arbitrated and indexed with semester periods. It supports a wide range of contents that are evaluated by academic peers by the Double-Blind method, around subjects related to the theory and practice of image and signal processing, control-digital system-artificial, intelligence-fuzzy, logic-mathematical, modeling-computational, mathematics-computer, science with diverse approaches and perspectives , That contribute to the diffusion of the development of Science Technology and Innovation that allow the arguments related to the decision making and influence in the formulation of international policies in the Field of Physical Sciences Mathematics and Earth sciences. The editorial horizon of ECORFAN-Mexico® extends beyond the academy and integrates other segments of research and analysis outside the scope, as long as they meet the requirements of rigorous argumentative and scientific, as well as addressing issues of general and current interest of the International Scientific Society.

Editorial Board

Arbitration Committee

Assignment of Rights

The sending of an Article to ECORFAN-Democratic Republic of Congo emanates the commitment of the author not to submit it simultaneously to the consideration of other series publications for it must complement the Originality Format for its Article.

The authors sign the Authorization Format for their Article to be disseminated by means that ECORFAN-Mexico, S.C. In its Holding Democratic Republic of Congo considers pertinent for disclosure and diffusion of its Article its Rights of Work.

Declaration of Authorship

Indicate the Name of Author and Coauthors at most in the participation of the Article and indicate in extensive the Institutional Affiliation indicating the Department.

Identify the Name of Author and Coauthors at most with the CVU Scholarship Number-PNPC or SNI-CONACYT- Indicating the Researcher Level and their Google Scholar Profile to verify their Citation Level and H index.

Identify the Name of Author and Coauthors at most in the Science and Technology Profiles widely accepted by the International Scientific Community ORC ID - Researcher ID Thomson - arXiv Author ID - PubMed Author ID - Open ID respectively.

Indicate the contact for correspondence to the Author (Mail and Telephone) and indicate the Researcher who contributes as the first Author of the Article.

Plagiarism Detection

All Articles will be tested by plagiarism software PLAGSCAN if a plagiarism level is detected Positive will not be sent to arbitration and will be rescinded of the reception of the Article notifying the Authors responsible, claiming that academic plagiarism is criminalized in the Penal Code.

Arbitration Process

All Articles will be evaluated by academic peers by the Double Blind method, the Arbitration Approval is a requirement for the Editorial Board to make a final decision that will be final in all cases. MARVID® is a derivative brand of ECORFAN® specialized in providing the expert evaluators all of them with Doctorate degree and distinction of International Researchers in the respective Councils of Science and Technology the counterpart of CONACYT for the chapters of America-Europe-Asia-Africa and Oceania. The identification of the authorship should only appear on a first removable page, in order to ensure that the Arbitration process is anonymous and covers the following stages: Identification of the Journal with its author occupation rate - Identification of Authors and Coauthors - Detection of plagiarism PLAGSCAN - Review of Formats of Authorization and Originality-Allocation to the Editorial Board- Allocation of the pair of Expert Arbitrators-Notification of Arbitration - Declaration of observations to the Author-Verification of Article Modified for Editing-Publication.

Instructions for Scientific, Technological and Innovation Publication

Knowledge Area

The works must be unpublished and refer to topics of Image and signal processing, control-digital system-artificial, intelligence-fuzzy, logic-mathematical, modeling-computational, mathematics-computer, science and other topics related to Physical Sciences Mathematics and Earth sciences.

Presentation of the Content

In the first article we present, *Use of metallic nanoparticles for characterization of muscle tissue by electrical impedance spectroscopy (EIS)*, by MORENO GONZÁLEZ-TERAN, Gustavo, CEJA-FERNANDEZ, Andrea, GALINDO-GONZÁLEZ, Rosario and BALLEZA-ORDAZ, José Marco, with adscription in the Universidad de Guanajuato, as the next article we present, *Structural and thermoelectric properties of the* $Pr_2Zr_2O_7$ *compound*, by QUIROZ-RODRÍGUEZ, Adolfo, GUARNEROS-AGUILAR, Cesia and AGUSTIN-SERRANO, Ricardo, with adscription in the Universidad Tecnológica de Xicotepec de Juárez, CONACYT- Instituto Politécnico Nacional and Benemérita Universidad Autónoma de Puebla, as the next article we present, *Dynamic Partial Encryption System for Digital Image*, by RODRIGUEZ-CARDONA, Gustavo, RAMIREZ-BELTRAN, Leonardo Humberto and RAMIREZ-TORRES, Marco Tulio, with adscription in the Universidad Autónoma de San Luis Potosí, as the next article we present, *Oscillation of a pendulum subject to a horizontal trajectory with different kinds of motion*, by ESPINDOLA-HEREDIA, Rodolfo, DEL VALLE, Gabriela, MUCIÑO-CRUZ, Damián and HERNANDEZ-MORALES, Guadalupe, with adscription in the Universidad Autónoma Metropolitana.

Content

Article **ECORFAN Journal Democratic Republic of Congo**
December 2019 Vol.5 No.9 1-3

Use of metallic nanoparticles for characterization of muscle tissue by electrical impedance spectroscopy (EIS)

Uso de nanopartículas metálicas para la caracterización del tejido muscular mediante espectroscopia de impedancia eléctrica (EIS)

MORENO GONZÁLEZ-TERAN, Gustavo[1]†, CEJA-FERNANDEZ, Andrea[1], GALINDO-GONZÁLEZ, Rosario[2] and BALLEZA-ORDAZ, José Marco[1]

[1] *Universidad de Guanajuato. División de Ciencias e Ingeniería.*
[2] *Universidad de Guanajuato. División de Ciencias Naturales y Exactas.*

ID 1st Author: *Gustavo, Moreno González-Teran* / **ORC ID:** 0000-0002-1959-1571

ID 1st Coauthor: *Andrea, Ceja-Fernandez* / **ORC ID:** 0000-0002-5595-6611

ID 2nd Coauthor: *Rosario, Galindo-González* / **ORC ID:** 0000-0002-3612-1555, **CVU CONACYT ID:** 223987

ID 3rd Coauthor: *José Marco, Balleza-Ordaz* / **ORC ID:** 0000-0002-3246-0277, **CVU CONACYT ID:** 406536

DOI: 10.35429/EJDRC.2019.9.5.1.3 Received July 26, 2019; Accepted September 23, 2019

Abstract

Objectives. The electrical impedance spectroscopy (EIS) is relatively new technique used in medicine. The main problems that should be solved are its low resolution and that it fails to distinguish between tissue types, so some kind of the contrast should be applied. Magnetical nanoparticles have been used for imaging and other medical applications. For that reason, our research group decided to analyse the changes of electrical properties of chicken muscle tissue caused by three different types of metal nanoparticles at 50KHz. Methodology. Bio-Logic Science Instruments SP-150 was used as EIS device. Three different particles were analysed: two types of nanomagnetite (NM1 and NM2) and one of Gold particles (GNP). NM1 and NM2 samples were synthetized by coprecipitation and combustion method, respectively. GNP were synthetized by Turkevich method. Nanoparticles were characterized by SEM and RAMAN spectroscopy. Four needles were placed in each chicken breast to connect the EIS device. Measurements were obtained from each chicken breast at basal stage and after being injected with nanoparticles. Data was analyzed by bode graphics (module and phase). Contribution. The major changes of electrical properties of tissue were evidenced by using NM1 and GNP.

Magnetite, Gold nanoparticles, Electrical impedance

Resumen

Objetivos. La espectroscopia de impedancia eléctrica (EIS) es una técnica utilizada en medicina. Los principales problemas que deben resolverse son su baja resolución y el no poder distinguir entre los tipos de tejido, por lo tanto, se necesita aplicar un medio de contraste. Las nanopartículas magnéticas se han usado en imagenología y otras aplicaciones médicas. Por esa razón, nuestro grupo de investigación decidió analizar los cambios en las propiedades eléctricas del tejido muscular del pollo causados por tres tipos diferentes de nanopartículas metálicas a 50KHz. Metodología. Bio-Logic Science Instruments SP-150 se utilizó como dispositivo EIS. Se analizaron tres partículas: dos de nanomagnetita (NM1 y NM2) y una de oro (GNP). Las muestras de NM1 y NM2 se sintetizaron por los métodos de coprecipitación y de combustión, respectivamente. El GNP se sintetizó mediante el método de Turkevich. Las nanopartículas se caracterizaron por SEM y espectroscopia RAMAN. Se colocaron cuatro agujas en cada pechuga de pollo para conectar el dispositivo. Las mediciones se obtuvieron de cada pechuga de pollo antes y después de ser inyectadas con nanopartículas. Los datos fueron analizados por gráficos de Bode (módulo y fase). Las diferencias más significativas se muestran usando las partículas NM1 Y GNP. Contribución. Los principales cambios en las propiedades eléctricas en el tejido se evidenciaron mediante el uso de NM1 y GNP.

Magnetita, Nanopartículas de oro, Impedancia eléctrica

Citation: MORENO GONZÁLEZ-TERAN, Gustavo, CEJA-FERNANDEZ, Andrea, GALINDO-GONZÁLEZ, Rosario and BALLEZA-ORDAZ, José Marco. Use of metallic nanoparticles for characterization of muscle tissue by electrical impedance spectroscopy (EIS). ECORFAN Journal-Democratic Republic of Congo. 2019, 5-9: 1-3.

† Researcher contributing first author.

Introduction

The electrical impedance spectroscopy (EIS) is a versatile technique that consist in injection of an electrical current and detection of potential and *vice versa*. Applications of this technique include but are not limited to materials characterization, exploration of cavities in constructions, transmission lines and medicine.

Medical application of EIS is based on the fact that it allows to characterize the electrical properties of tissues by detecting volume changes and the variations of cellular structure. Electrical current used for this purpose is very small and undetected for human body (less then 1mA), also electrical impedance equipment is relatively cheap and can be produced as portable devices.

The main problem that should be solved in order to establish EIS as a reliable medical procedure is its low resolution and it fails to distinguish between tissue types, so some kind of the contrast should be applied.

Magnetic nanoparticles provide a multifunctional platform for scientific and clinical applications, such as biosensors, protein and cell separation systems and magnetic carriers for hyperthermia and tissue specific drug delivery. For instance, nanomagnetite was assessed as imaging contrast for magnetic resonance tomography with good results and as an agent for magnetically guided drug delivery. In other hand, the gold nanoparticles also have shown promising results in targeted drug delivery, imaging, photothermal and photodynamic therapy.

Taking into account that metallic nanoparticles possess electrical properties different from living tissue our research group decided to assess them in EIS measurements. In this work, changes of the parameters of impedance vector (module and phase) in three chicken breasts under the influence of three different nano-particles (two samples of nanomagnetite synthetized by two different methods and one sample of nanogold particles synthesised by precipitation method) were assessed. At this work we present the results at 50 KHz frequency, of interest at our group, at which a change in the cellular structure can be detected.

Methodology

For this work a Bio-Logic Science Instruments SP-150 was used as EIS device. Three chicken breasts were used, weighing 345.9 g, 349.5 g 270g. Each one was analyzed at basal state an under the influence of a specific nanoparticle.

Three types of nanoparticle were used: two nanomagnetite (NM1, NM2) synthetized by coprecipitation and combustion method, respectively; the NM1 particle, exhibited a hematite phase; a gold particle (GNP) synthetized by Turkevich method.

The nanomagnetite particles were characterized by SEM and Raman spectroscopy.

Four needles (38mm) were placed in each chicken breast to connect the EIS device.

Five measurements were obtained from each chicken breast at: I) basal stage II) after being injected with nanoparticles, the equipment setting is shown in Figure 1.

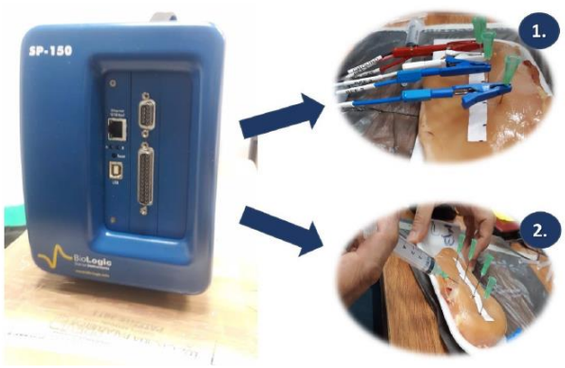

Figure 1 EIS device (left) connected to chicken breast at 1) basal stage and 2) after being injected with nanoparticles

The impedance measurements were made at 50 KHz and the mean value of the impedance-module an impedance-phase was calculated, for each chicken breast.

All the parameters of impedance vector were analyzed by Bode graphics (magnitude and phase).

ISSN 2414-4924

Results

The particle size of NM1 is 10-70 nm. Similarly, NM2 sample's particles were irregular in shape with size less than 100 nm. GNPs were colloidally suspended with size 10-50 nm. RAMAN spectra of synthetized nanoparticles are shown in Figure 2. It can be observed that nanomagnetite synthesized by two methods shows similar RAMAN spectra, so it can be concluded that this two samples possess similar composition.

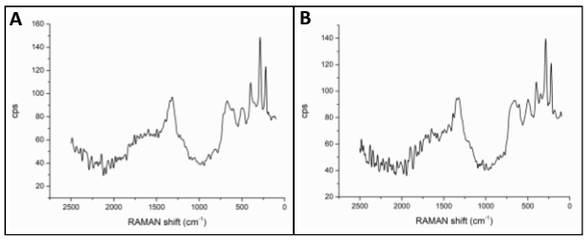

Figure 2 RAMAN spectra of used nanoparticles: A) NM1; B) NM2

The mean value of impedance-module and impedance-phase at basal stage and under the influence of the three nanoparticles were for breast 1 (NM1): 244.1Ω (-58.47°) and 147.5Ω (-47.8°), for breast 2 (NM2): 141.4Ω (-47.7°) and 138.9Ω (-47.6°), for breast 3 (GNP): 130.9Ω (-38.1°) and 132.9Ω (-39.1°), respectively.

Conclusions

The major changes of electrical properties of chicken breast were evidenced by using NM1 and GNP due to the particle size, NM1 phase condition, and Au conductivity. For the further evaluation of use of nanoparticles in EIS technique, they should be evaluated in other tissue types.

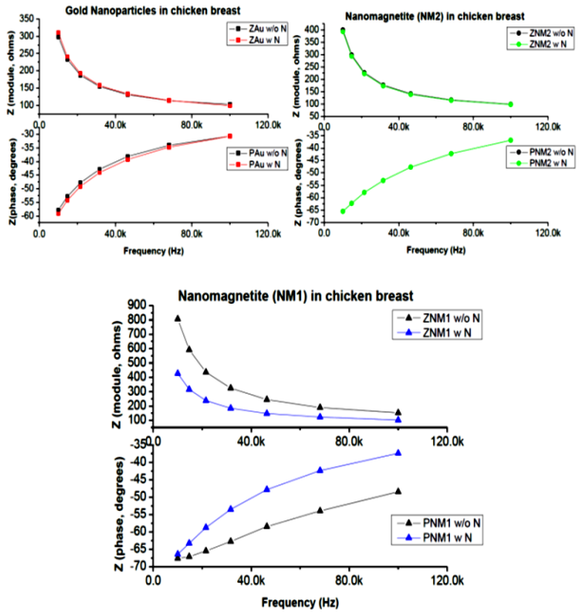

Figure 3 Graph of impedance vector (magnitude and phase) at 1) basal stage and 2) after being injected with nanoparticles (GNP, NM1, NM2)

References

Kyle, U. G., Bosaeus, I., De Lorenzo, A. D., Deurenberg, P., Elia, M., Gómez, J. M., ... & Scharfetter, H. (2004). Bioelectrical impedance analysis—part I: review of principles and methods. Clinical nutrition, 23(5), 1226-1243.

Vilos, C., Gutiérrez, M., Escobar, R. A., Morales, F., Denardin, J. C., Velasquez, L., & Altbir, D. (2013). Superparamagnetic Poly (3-hydroxybutyrate-co-3 hydroxyvalerate) (PHBV) nanoparticles for biomedical applications. Electronic Journal of Biotechnology, 16(5), 8-8.

ISSN 2414-4924

Article **ECORFAN Journal-Democratic Republic of Congo**
December 2019 Vol.5 No.9 4-9

Structural and thermoelectric properties of the $Pr_2Zr_2O_7$ compound

Propiedades estructurales y termoeléctricas del compuesto $Pr_2Zr_2O_7$

QUIROZ-RODRÍGUEZ, Adolfo[1]†*, GUARNEROS-AGUILAR, Cesia[2] and AGUSTIN-SERRANO, Ricardo[3]

[1]Universidad Tecnológica de Xicotepec de Juárez, Industrial and Petroleum Maintenance Area. Av. Universidad Tecnológica No. 1000, Col. Tierra Negra, Cd. Xicotepec de Juárez, Pue., México. C.P. 73080
[2]CONACYT- Instituto Politécnico Nacional, Materials and Technologies for Energy Health and Environment (GESMAT), CICATA Altamira, Km 14.5 Street Tampico-Puerto Industrial Altamira, Altamira, Tamaulipas, México. C. P. 89600
[3]Benemérita Universidad Autónoma de Puebla. Faculty of Mathematical Physical Sciences, Av. San Claudio y 18 Sur, Ciudad Universitaria, Puebla, Pue. México. C. P. 72570

ID 1st Author: *Adolfo, Quiroz-Rodríguez* / **ORC ID:** 0000-0002-9685-9455, **arXiv Author ID:** adolfo-79, **CVU CONACYT ID:** 105471

ID 1st Coauthor: *Cesia, Guarneros-Aguilar* / **ORC ID:** 0000-0001-8751-4394, **CVU CONACYT ID:** 46832

ID 2nd Coauthor: *Ricardo, Agustin-Serrano* / **ORC ID:** 0000-0002-6468-7548, **CVU CONACYT ID:** 165478

DOI: 10.35429/EJDRC.2019.9.5.4.9 Received July 28, 2019; Accepted September 25, 2019

Abstract

In this research, it is presented a detailed study of the structural and thermoelectric properties of the pyrochlore zirconium $Pr_2Zr_2O_7$ compound prepared by solid-state reaction (SSR) in air at ambient pressure. The synthesized sample was characterized using powder X-ray diffraction. The thermal stability of the thermoelectric compound (TE) $Pr_2Zr_2O_7$ was tested by thermogravimetric analysis (TGA) and differential thermal analysis (DTA). Scanning electron microscopy shows that the crystal size varies between 0.69 and 2.81μm. Electrical conductivity (σ) of the sample calcined at 1400 °C presented values increase irregularly with the increasing temperature from 0.001 to 0.018 S cm^{-1} as expected in a semiconductor material. The thermal conductivity is lower than 0.44 - 775 W m^{-1} K^{-1} which is quite anomalous in comparison with the thermal conductivity of other oxides.

Solid-state reaction, Pyrochlore compounds, Crystal structure

Resumen

En esta investigación, se presenta un estudio detallado de las propiedades estructurales y termoeléctricas del compuesto pirocloro de circonio $Pr_2Zr_2O_7$ preparado por reacción en estado sólido (SSR) en aire a presión ambiente. La muestra sintetizada se caracterizó utilizando difracción de rayos-X en polvo. La estabilidad térmica del compuesto termoeléctrico (TE) $Pr_2Zr_2O_7$ se probaron mediante análisis termogravimetrico (TGA) y análisis térmico diferencial (DTA). Microscopía electrónica de barrido muestra que el tamaño del cristal varía entre 0.69 y 2.81μm. La conductividad eléctrica (σ) de la muestra calcinada a 1400 ° C presentó valores que aumentan irregularmente con el aumento de la temperatura de 0.001 a 0.018 Scm^{-1} como se esperaba en un material semiconductor. La conductividad térmica es inferior a 0.44 - 775 W m^{-1} K^{-1} , lo cual es bastante anómalo en comparación con la conductividad térmica de otros óxidos.

Reacción en estado sólido, Compuestos de pirocloro, Estructura cristalina

Citation: QUIROZ-RODRÍGUEZ, Adolfo, GUARNEROS-AGUILAR, Cesia and AGUSTIN-SERRANO, Ricardo. Structural and thermoelectric properties of the $Pr_2Zr_2O_7$ compound. ECORFAN Journal-Democratic Republic of Congo. 2019, 5-9: 4-9

* Correspondence to Author (email: adolfo.quiroz@utxicotepec.edu.mx)
† Researcher contributing first author.

Introduction

Thermoelectric devices are a technology that converts waste heat into electric power or vice versa through the thermoelectric phenomena in semiconductor solids [1]. Since this technology is a direct energy conversion in solids, it has attracted a renewed interest as a fundamental technology for environmentally friendly energy conversion. In particular, thermoelectric power generation has been now considered as a possible renewable energy source. The thermoelectric materials comprises from semimetals, semiconductors, ceramics to polymers. However, thermoelectric oxide materials have been extensively investigated as a promising thermoelectric power generator because they are stable at high temperatures in air. Oxides were considered to be poor thermoelectric materials, but after the discovery of a large thermoelectric power factor in Na_xCoO_2, some cobalt oxides are recognized as good p-type thermoelectric oxides [2,3]. In contrast, not yet discovered is an n-type counterpart to the cobalt oxides. Some of the transparent conductors such as ZnO and In_2O_3 show indeed good thermoelectric performance above 1000 K, [4,5] but the lattice thermal conductivity is much higher than the conventional thermoelectric materials. The doped titanates [6,7] and niobates [8-10] are fairly good n-type thermoelectric materials at room temperature, but they are easily oxidized at high temperature to lose conductivity in air. Recently, a large Seebeck coefficient and low thermal conductivity have been reported in polycrystalline samples of the double perovskite ruthenate Sr_2LRuO_6 (L; rare-earth) [11]. Although the magnetic properties and ground states of the titanate pyrochlores have been investigated in detail, similar studies of the zirconate pyrochlores have been hampered by the lack of large, good quality single crystals. With the exception of a few investigations on $Pr_2Zr_2O_7$ single crystals [12-14], most of the research on the zirconate pyrochlores has used powder samples [15-22].

The aim of this investigation was to synthe- size the polycrystaline $Pr_2Zr_2O_7$ compound via the solid-state reaction method and a detailed study of the precise time for obtaining the compound. In the present contribution, we report the relationship between structural, Seebeck Coefficient, electrical conductuvity and termal conductivity properties of the pirochlore $Pr_2Zr_2O_7$.

These properties make rare-earth zirconates suitable for a variety of applications such as solid electrolytes, catalysts, nuclear waste forms, and especially high-temperature TBCs (Thermal barrier coatings) materials [23].

Materials and Methods

Polycrystalline sample of the $Pr_2Zr_2O_7$ compound was synthesized by solid-state reaction at ambient pressure in air. The starting materials were ZrO_2 (Riedel-de Haën pure), and Pr_2O_3 (Cerac, 99.9 %). Structure and purity of the materials were determined by XDR. The stoichiometric mixture of the starting materials was done in air during 30 minutes, agrided with an agata mortar, resulting in homogenous slurry [24].

The resultant $Pr_2Zr_2O_7$ mixture was compressed into pellets (13 mm diameter, 1.0-1.5 ± 0.05 mm thickness) by applying a pressure of 3 tons/cm^2 during 5 minutes under vacuum. The resulting compacted specimens were then sintered in air at 1400 °C during 3 days and then cooled down to room temperature following the natural cooling of furnace to 7 h.

The thermal behavior of $Pr_2Zr_2O_7$ compound was studied from 25 to 1200 °C through differential thermal analysis (DTA), and thermogravimetric analysis (TGA) using measuring equipment SDT Q600, TA Instruments. Sample was characterized by X-ray powder diffraction (XRD) using an APD 2000 diffractometer with Cu Kα radiation (λ = 1.5406 *Å*) and a graphite monocromator.

Diffraction patterns were collected at room temperature in air, over the 2θ range 10º – 90º with a step size of 0.025º and a time per step of 15 seconds. Changes in morphology and grain size were induced in the sample by performing different heat treatments during all the process of the sample preparation and examined by scanning electron microscopy (SEM) on a Hitachi S-3400N-II System.

The 10.00 K.X micrograph was taken with a voltage of 20 kV, a current intensity of 1000 pA and WD = 10 mm. Energy Dispersive X-Ray (EDX) was performed on the same SEM system, which is equipped with an EDAX 9900 device.

ISSN 2414-4924

For thermoelectric characterization, square-shaped compact of dimension 10 mm x 10 mm x 0.5 mm was prepared using a 3-ton hydraulic press, Seebeck coefficient and electric conductivity were measured simultaneously under a 10 sscm N_2 flux, from 100 to 800 °C in a high- precision SBA 458 Nemesis Netzsch system imposing a 0.05 A current; the heater voltage for Seebeck measurements was 1.0 V, the temperature increment was 5 Ks $^{-1}$, and the temperature difference threshold is 15 K. The thermal conductivity was measured in a LFA 467 HyperFlash Netzsch apparatus equipped with a xenon flash lamp and an InSb detector, in the temperature range from 100 to 600 °C, with pulsed energy up to 10 J/pulse and pulse width of 20–1200 μs.

Results and Discussions

Thermogravimetric Analysis (TGA). The TGA curves are important to determine the temperatures to which the formation of organic matter and subproducts take place during the solid-state reaction method. The results obtained from this technique did help to control the process parameters to produce the $Pr_2Zr_2O_7$ compound. The TGA results obtained from the $Pr_2Zr_2O_7$ were analyzed separately and are shown in Figure 1. The TGA (a) curve is divided in three most relevant regions: 25-350 °C, 350–700 °C, and 700-1200 °C. In the next ascend TGA curve start with a hydrated material at room temperature up to 350 °C. After 350 °C an increase in curve means, the formation of $Pr_2Zr_2O_7$ compound (seen in some reaction conditions by XRD). Around 700 °C it is detected a weak lost of energy peak that may be due to the melting of reagents, binary and ternary compounds corroborated by XRD.

The DTA (b) curve for $Pr_2Zr_2O_7$ compound is presented in Figure 1. The sample present a first exothermic effect around 300 °C, which is unusual; it means that the strcuture that is obtained between 300 and 1200 °C is metaestable and the DTA exotherm signs a decrease in enthalpy of the sample and therefore a change to a more stable structure. For temperatures higher than 1200 °C, exothermic effects are observed that are important to understand the stability in the solid solution formation mechanism as its thermal stability.

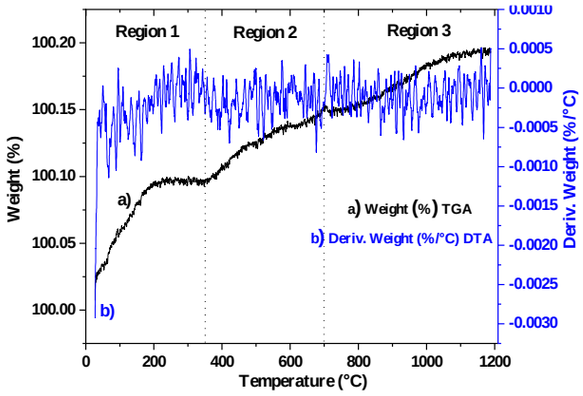

Figure 1 TGA and DTA of the $Pr_2Zr_2O_7$ sample

Figure 2 presents the X-ray diffraction pattern of the sintered $Pr_2Zr_2O_7$ compound. The combination of the XRD and TGA analysis proved to be useful when observing the number of phases that changed during the applied heat treatments to $Pr_2Zr_2O_7$ sample. The solid line corresponds to a cubic polycrystalline phase with $Fd\bar{3}m$ (No. 227) space group and it is identified as $Pr_2Zr_2O_7$ compound with PDF (04-008-6354).

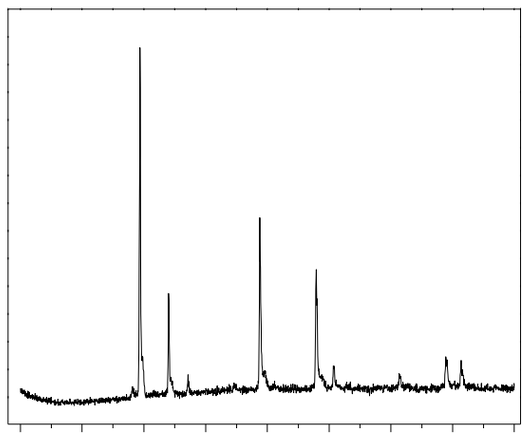

Figure 2 XRD Pattern evolution of pyrochlore $Pr_2Zr_2O_7$ compound

The EDX elemental analysis of the $Pr_2Zr_2O_7$ compound is shown in Figure 3. The atomic percentage for the Pr, Zr and O was 54.14%, 28.11% and 19.75%, respectively.

ISSN 2414-4924

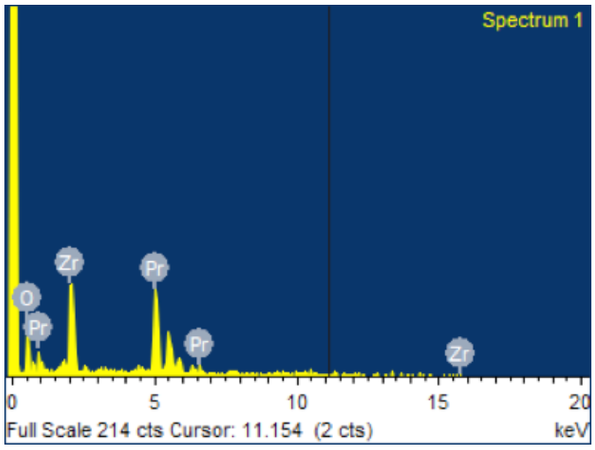

Figure 3 Spectrum of EDX analysis for the $Pr_2Zr_2O_7$ compound after applying the heat treatment at 1400 ° C during 3 days

Figure 4 shows the elemental SEM mapping performed to the produced $Pr_2Zr_2O_7$ compound. This analysis confirmed the homogeneous distributions of the $Pr_2Zr_2O_7$ compound in the sample. The sample calcined at 1400 °C shows the formation of different particle sizes between 0.69 and 2.81 μm, and some of them present a well-defined grain boundary, while the rest are agglomerations.

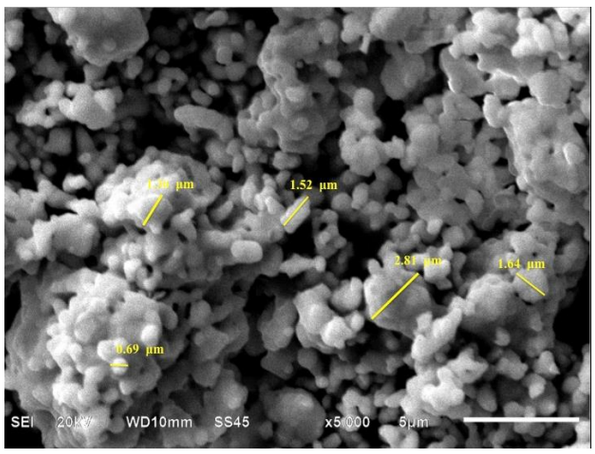

Figure 4 SEM for the $Pr_2Zr_2O_7$ compound

Electrical conductivity (σ) of the sample calcined at 1400 °C is presented in Figure 5. Sample calcined at 1400 °C show a electrical conductivity low. The σ values increase irregularly with the increasing temperature from 0.001 to 0.018 Scm^{-1} as expected in a semiconductor material [25].

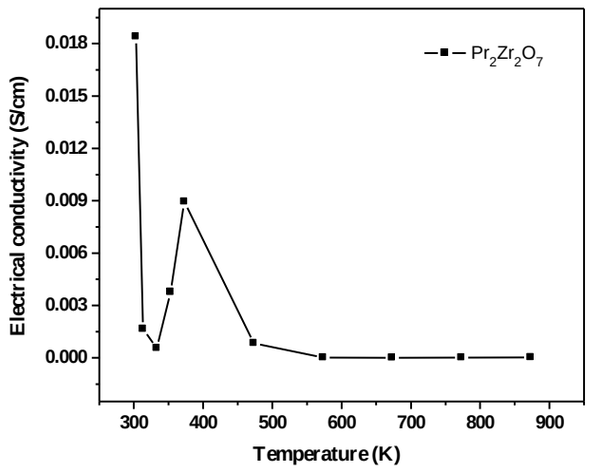

Figure 5 Temperature dependence of electrical conductivity for $Pr_2Zr_2O_7$ sample obtained at 1400 °C

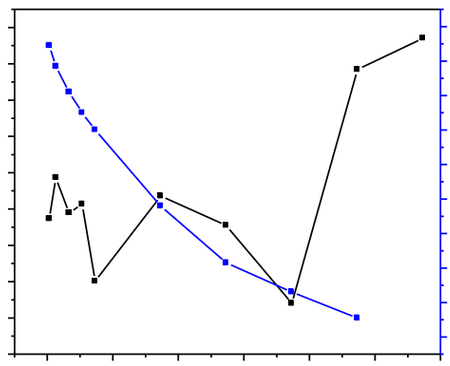

Figure 6 Seebeck coefficient and thermal conductivity in the temperature range 300–900 °K

Seebeck coefficient and thermal conductivity measured as a function of temperature are presented in Figure 6. The Fig. 6 (a) show S values, ranging from -0.00025 to 0.0005 μVK^{-1}, are positive and negative over the temperature range confirming the semiconductor p and n-character, where the holes and electrons are the main charge carriers. The p-character in $Pr_2Zr_2O_7$ has been attributed to the deviation from stoichiometric composition and ionized and / or interstitial oxygens generate positive holes [26-28].

The sign for the sample is negative, and the magnitude systematically decreases with increasing temperature. These results show that the Pr^{+3} ion acts as a donor to supply electrons to the system. The calculated thermal conductivity of Pr2 Zr2O7 ceramic as a function of temperature are plotted in Fig. 6 (b). The thermal conductivity of Pr2Zr2O7 ceramic gradually decrease with the increase of temperature up to 800° C, which is attributed to the lattice thermal conduction.

ISSN 2414-4924

Acknowledgments

The authors acknowledge the financial support provided by Universidad Tecnológica de Xicotepec de Juárez and Karla Eriseth Reyes Morales form Instituto de Investigaciones en Materiales of Universidad Nacional Autónoma de México, for performing thermogravimetric analysis (TGA) measurements. SBA 458 Nemesis and LFA 467 HyperFlash Netzsch systems were acquired by Project 252705 from CONACYT INFR-2015-01. The authors acknowledge to MTA Juan Jesús Reyes for Seebeck coefficient and thermal conductivity measurements.

Conclusion

In this work, was obtained polycrystalline $Pr_2Zr_2O_7$ compound by solid-state reaction method in air at atmospheric pressure. SEM micrograph shows the effect of heat treatments and processing route on the grain morphology of the compound. The σ values increase irregularly with the increasing temperature from 0.001 to 0.018 Scm^{-1} as expected in a semiconductor material.

Perspectives

As future considerations, with the result of the measurements obtained in this study we have as future research to improve the electrical conductivity property of our new compounds using small quantities of Sr^{+2} doping and to decrease the thermal conductivity, which will help us obtain a zirconium pyrochloro with better thermoelectric properties for applications in solid electrolytes, catalysts, nuclear waste forms, and especially high-temperature TBC materials.

References

[1] Mahan, G. (1997). Good thermoelectrics. Solid state physics, 51, 81-157.

[2] Terasaki, I., Sasago, Y., and Uchinokura, K. (1997). Large thermoelectric power in $NaCo_2O_4$ single crystals. Phys. Rev. B 56, R12685.

[3] Takahata, K., Iguchi, Y., Tanaka, D., Itoh, T., and Terasaki, I. (2000). Low thermal conductivity of the layered oxide $(Na,Ca)Co_2O_4$: Another example of a phonon glass and an electron crystal. Phys. Rev. B 61, 12551.

[4] Ohtaki, M., Tsubota, T., Eguchi, K., and Arai, H. (1996). Hightemperature thermoelectric properties of $(Zn_{1-x}Al_x)O$. J. Appl. Phys. 79, 1816.

[5] Bérardan, D., Guilmeau, E., Maignan, A., and Raveau, B. (2008). Enhancement of the thermoelectric performances of In_2O_3 by the coupled substitution of M^{2+}/Sn^{4+} for In^{3+}. J. Appl. Phys. 104, 064918.

[6] Okuda, T., Nakanishi, K., Miyasaka, S., and Tokura, Y. (2001). Large thermoelectric response of metallic perovskites: $Sr_{1-x}La_xTiO_3(0<\sim x<\sim 0.1)$. Phys. Rev. B 63, 113104.

[7] Ohta, S., Nomura, T., Ohta, H., and Koumoto, K. (2005). High-temperature carrier transport and thermoelectric properties of heavily La- or Nb-doped $SrTiO_3$single crystals. J. Appl. Phys. 97, 034106.

[8] Sakai, A.,Kannon, T.,Takahashi, K., Yamada, Y.,Adachi, H. (2010).Large anisotropic thermoelectricity in perovskite related layered structure: $SrnNbnO_{3n+2}$, n = 4, 5

[9] Kobayashi, W., Hayashi, Y., Matsushita, M., Yamamoto, Y., Terasaki, I., Nakao, A., Nakao, H., Murakami, Y., Moritomo Y., and Karppinen, M. (2011) Anisotropic thermoelectric properties associated with dimensional crossover in quasi-one-dimensional $SrNbO_{3.4+d}$ (d ~ 0.03). Phys. Rev. B 84, 085118.

[10] Lee, S., Dursun, S., Duran C., and Randall, C. A. (2011).Thermoelectric power factor enhancement of textured ferroelectric $Sr_xBa_{1-x}Nb_2O_{6-\delta}$ ceramics. J. Mater. Res. 26, 26.

[11] Aguirre, M. H., Logvinovich, D., Bocher, L., Robert, R., Ebbinghaus, S. G., and Weidenkaff, A. (2009). High-temperature thermoelectric properties of Sr_2RuYO_6 and Sr_2RuErO_6 double perovskites influenced by structure and microstructure. Acta Mater. 57,108.

[12] Matsuhira K, Sekine C, Paulsen C, Wakeshima M, Hinatsu Y, Kitazawa T, Kiuchi Y, Hiroi Z and Takagi S. (2009). Spin freezing in the pyrochlore antiferromagnet $Pr_2Zr_2O_7$. J. Phys.: Conf. Ser. 145 012031.

ISSN 2414-4924

[13] Kimura, K., Nakatsuji, S., Wen, J-J, Broholm, C., Stone, M. B., Nishibori, E., and Sawa, H. (2013). Quantum fluctuations in spin-ice-like $Pr_2Zr_2O_7$. Nat. Commun. 4 1934

[14] Kimura, K., and Nakatsuji, S. (2013). Single-crystal study on the low-temperature magnetism of the pyrochlore magnet $Pr_2Zr_2O_7$. J. Korean Phys. Soc. 63 719.

[15] Koteswara Rao K., Banu T., Vithal M., Swamy G. Y. S. K., and Ravi Kumar K. (2002). Preparation and characterization of bulk and nano particles of $La_2Zr_2O_7$ and $Nd_2Zr_2O_7$ by sol–gel method Mater. Lett. 54 205.

[16] Lutique S, Javorský P, Konings R J M, van Genderen A C G, van Miltenburg J C and Wastin F. (2003). Low temperature heat capacity of $Nd_2Zr_2O_7$ pyrochlore. J. Chem. Thermodynamics 35 955.

[17] Zhang F X, Lian J, Becker U, Wang L M, Hu J, Saxena S and Ewing R C. (2007). Structural distortions and phase transformations in $Sm_2Zr_2O_7$ pyrochlore at high pressures. Chem. Phys. Lett. 441 216.

[18] Singh S, Saha S, Dhar S K, Suryanarayanan R, Sood A K and Revcolevschi A. (2008). Manifestation of geometric frustration on magnetic and thermodynamic properties of the pyrochlores $Sm_2X_2O_7$ (X= Ti, Zr). Phys. Rev. B 77 054408.

[19] Radha A V, Ushakov S V and Navrotsky A (2009). Thermochemistry of lanthanum zirconate pyrochlore. J. Mater. Res. 24 3350

[20] Kopan A R, Gorbachuk M P, Lakiza S M and Tischchenko Y S. (2010). Low-temperature heat capacity of samarium zirconate ($Sm_2Zr_2O_7$). Powder Metall. Met. Ceram. 49 317

[21] Chiu C-W, Lee Y-H, Sheu H-S and Kao H-C I. (2010). Phase Transition and the Thermal Activated Ordering of the Ions with Pyrochlore Phase in $Ln_2Zr_2O_7$ (Ln = Sm, Eu) J. Chinese Chem. Soc. 57 925

[22] Blanchard P. E. R., Clements R, Kennedy B J, Ling C D and Reynolds E. (2012). Investigating the order–disorder phase transition in $Nd_{2-x}Y_xZr_2O_7$ via diffraction and spectroscopy. Inorg. Chem. 51 13237

[23] Subramanian M. A., Aravamudan G., and Subba Rao G. V. (1983) ‘‘Oxide Pyrochlores–A Review,’’ Prog. Solid State Chem., 15 55–143.

[24] Quiroz A, Chavira E, Garcia-Vazquez V, Gonzalez G, and Abatal M. (2018). Structural, electrical and magnetic properties of the pyrochlorate. $Er_{2-x}Sr_xRu_2O_7$ ($0 \leq x \leq 0.10$) system. Revista Mexicana de Fısica 64 (3) 222–227.

[25] Neamen, D.A. (2012). Semiconductor physics & devices: basic principles, 4th edn. McGraw-Hill, New York.

[26] Lu, Y., Nozue, T., Feng, N., Sagara, K., Yoshida, H., Jin, Y. (2015). Fabrication of thermoelectric CuAlO2 and performance enhancement by high density. J. Alloys Compd. 650:558–563.

[27] Park. K, Ko, KY, Seo, W. S. (2005) Thermoelectric properties of $CuAlO_2$. J. Eur. Ceram. Soc. 25:2219–2222.

[28] Tate, J., Ju, HL., Moon, J. C., Zakutayev, A., Richard, A. P., Russell, J., McIntyre, D. H. (2009). Origin of p-type conduction in single-crystal CuAlO2. Phys. Rev. B. 80:165206.

ISSN 2414-4924

Article **ECORFAN Journal-Democratic Republic of Congo**
December 2019 Vol.5 No.9 10-16

Dynamic Partial Encryption System for Digital Image

Sistema de Cifrado Parcial Dinámico para Imágenes Digitales

RODRIGUEZ-CARDONA, Gustavo†, RAMIREZ-BELTRAN, Leonardo Humberto and RAMIREZ-TORRES, Marco Tulio*

Universidad Autónoma de San Luis Potosí / Coordinación Académica Región Altiplano Oeste

ID 1st. Author: *Gustavo, Rodríguez- Cardona* / **ORC ID**: 0000-0002-5844-6254

ID 1st.Coauthor: *Leonardo Humberto, Ramírez- Beltrán* / **ORC ID**: 0000-0002-1044-425X

ID 2nd Coauthor: *Marco Tulio, Ramírez- Torres* / **ORC ID**: 0000-0002-7457-7318

DOI: 10.35429/EJDRC.2019.9.5.10.16 Received July 28, 2019; Accepted December 20, 2019

Abstract

The present investigation is proposing a new partial encryption algorithm for digital image, using the synchronization of cellular automata based on the local rule 90. Unlike other partial encryption algorithm, which become vulnerable to attacks such as Replacement Attack or Reconstruction Attack, this system encodes different bit planes, in function of the secret key, that is, for each block of clear text, different bits are encrypted to prevent that with an elimination operation of the encrypted bits information can be revealed. The synchronization of cellular automata has proven to be a useful tool for data encryption because it is sensitivity to initial conditions and, in addition, rule 90 is considered a chaotic standard. Both characteristics ensure cryptographic and perceptive security. Based on the results of the security analysis, this research could be an attractive option for image encryption with less computer cost and without compromising information confidentiality.

Cellular automata, Rule 90, Chaotic

Resumen

En la presente investigación se propone un nuevo algoritmo de cifrado parcial para imágenes digitales, utilizando la sincronización de autómatas celulares basada en la regla local 90. A diferencia de otros algoritmos de cifrado parcial, los cuales llegan a ser vulnerables a ataques como Replacement Attack o Reconstruction Attack, este sistema cifra diferentes planos de bits, en función de la clave secreta, es decir, para cada bloque de texto en claro se cifran diferentes bits, para evitar que con una operación de eliminación de los bits cifrados se pueda revelar información. La sincronización de autómatas celulares ha demostrado ser una herramienta útil para el cifrado de datos, debido a su sensibilidad a condiciones iniciales y a que la regla 90 es considerada de patrón caótico, ambas características permiten cumplir con la seguridad criptográfica y perceptual. Con base en los resultados del análisis de seguridad, esta propuesta podría ser una opción atractiva para cifrado de imágenes con un menor costo computacional sin comprometer la confidencialidad de la información.

Autómatas celulares, Regla 90, Caótico

Citation: RODRIGUEZ-CARDONA, Gustavo, RAMIREZ-BELTRAN, Leonardo Humberto and RAMIREZ-TORRES, Marco Tulio. Dynamic Partial Encryption System for Digital Image. ECORFAN Journal-Democratic Republic of Congo. 2019, 5-9: 10-16

* Correspondence to Author (email: tulio.torres@uaslp.mx)
† Researcher contributing first author.

Introduction

Nowadays is more common that we perform more operations via internet, thus facilitating processes and optimizing time. However, this means that users require more security and protection in the transmission of personal data, since these files are exposed in transmission links. One of the techniques used to protect information is encryption systems. This technique consists on making the information unintelligible in such a way that it can only be retrieved using the correct algorithm key.

Currently, image encryption is a very active area of research due to the high demand of multiple tasks where it is required, for example: videoconferences, satellite communications, video surveillance, medical imaging systems, among others. Although there are already several conventional encryption algorithms, such as AES (Advanced Encryption Standard) and DES (Data Encryption Standard), they have often been impractical and insecure in some ways for image encryption due to their intrinsic properties, such as high data rate, strong adjacent correlation, etc (Lian s, 2008). That is the reason why security problems expands every day, since encryption algorithms must provide perceptual and cryptographic security.

To avoid high latency in the encryption system, one option is to use partial encryption algorithms. This type consists on the encryption of a specific number of bits of the clear text block, while the rest remain unchanged. All of the above results in the investigation and implementation of new image encryption schemes, such as dynamic systems based on non-linear systems. That is why this research proposes a partial encryption system based on the synchronization of cellular automata using rule 90, which is classified as a chaotic pattern. The evaluation allows us to conclude that it is a strong algorithm against cryptanalysis and statistical attacks (Espinoza, 2018).

Foundations

Cellular Automata

Cellular automata (CA) emerged in the 1940s by mathematician John Von Neumann (Von, 1966), who tried to model a machine that was capable of self-replication.

Cellular automata consist of an ordered set of cells, in the form of a grid, where each cell has a finite number of states. The cellular automatons form a two-dimensional grid where their cells evolve in discrete steps, according to a local update rule applied uniformly, over all cells. At the beginning, a state is assigned to the cells at time t = 0, where the new states will depend on their previous states and those of their neighborhood, as shown in Fig. 1.

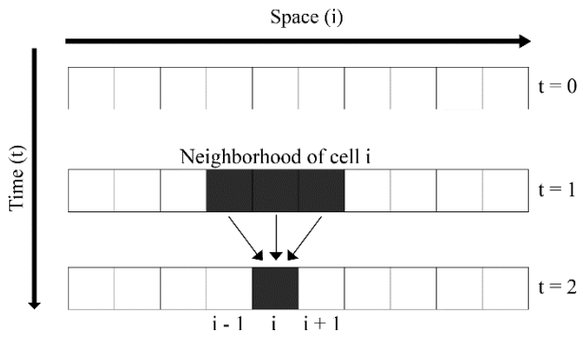

Figure 1 Space and Time Diagram of a cellular automaton
Source: Ramírez. (2015)

The assignment of values to all cells is known as configuration. The automaton receives an initial configuration and then progresses through other configurations in a sequence of discrete time steps. In each step all cells are updated simultaneously. A pre-specified rule determines the new value (Urias, 1998). This algorithm is used to calculate the next state of the cell.

Rule 90

Elemental Cellular Automata (ECA) differ from each other; just by choosing this local rule, they consider a neighborhood of radius 1, that is, a cell with its left and right neighbor. Each one can take only two values {0,1}, therefore there are only 8 combinations, resulting in 28 = 256 different local rules and ECA. Thus, local rule 90 is described by the expression of eq. (1):

$$X_i{}^{t+1} = (X^t{}_{i-1} + X^t{}_{i+1}) \; mod \; 2 \qquad (1)$$

In which X is the value in cell (0,1), $\boldsymbol{t}$ is the time and $\boldsymbol{i}$ is the index of its position. All cells obey the same rule, which can be given as a formula or as a table that specifies the new value for each possible combination of neighboring values. Rule 90 is one of the elementary rules of cellular automatons introduced by Stephen Wolfram in 1983 (Wolfram, 2018).

ISSN 2414-4924

The results of the rule are coded in the binary representation of the number 90 = 01011010.

Synchronization phenomenon

The synchronization phenomenon occurs after a period of time where the behaviors of two dynamic systems approach arbitrarily. The coupling of cellular automata occurs when a given set of coordinates (coupled coordinates) are copied from one of the systems, which is the cellular automaton known as the controller, in the system that will be called a replica. In this way, at each time step, both systems evolve with the same local rule and use the same coupled coordinates, thus synchronizing.

Next, in Fig. 2. we show a case considering n = 3, therefore the coupled coordinates are separated by $2^n - 1 = 7$ sites. In the same Fig. 2 we can see the evolution according to the rule 90 of cellular automatons of the controller and the replica with the same coupled coordinates. After $2^n - 1 = 7$ steps, the evolution of both cellular automata is the same (Urias, 1998).

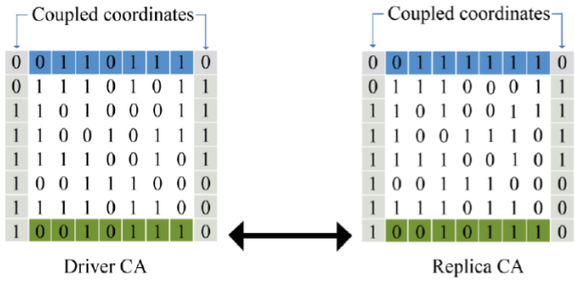

Figure 2 Synchronization phenomenon Left: CA controller. Right: CA replica
Source: Ramírez. (2015)

ESAC encryption system

The Synchronization System with Cellular Automata (SSCA) is a symmetric cipher that encrypts blocks of $\mathbf{2^k}$ -1 bit using for each block a subkey generated from an initial key. The SSCA system encrypts and decrypts a message divided into a sequence of 15-bit blocks, using a different key for each block. The same key must be used in the encryption and recovery of the original message.

The encryption mode requires a clear text block *p*, with size *L*, *p* will be the block to be encrypted. It also requires a random block *z*, with size *L + 1*, which will perform processing to *p*, and at the output it will have a processed data block $\hat{p}$. It also requires seeds that interact with each other to generate an encryption key *t* of size *N*. With this key, the data block is encrypted, obtaining the encrypted block *c*.

Based on the synchronization phenomena of the SSCA system, in ref. (Urias, 1998), the authors proposed a pseudorandom number generator (PRNG). Its main function is denoted as $h(\boldsymbol{p}, \boldsymbol{z})$and requires two vectors $\boldsymbol{p}$ and $\boldsymbol{z}$ of *n* bits and *n* + 1 bits, respectively. Where $\boldsymbol{p}$ is the pixel coefficient and $\boldsymbol{z}$ the random vector.

Pseudorandom Number Generator

Equations (2) for the generation of the key with N = 15 bits are shown below (Espinosa, 2018).

$$
\begin{aligned}
t1 &= x1 + y2 \\
t2 &= x2 + y1 + y3 \\
t3 &= x1 + x3 + y4 \\
t4 &= x4 + y1 + y3 + y5 \\
t5 &= x1 + x3 + x5 + y2 + y6 \\
t6 &= x2 + x6 + y1 + y5 + y6 \\
t7 &= x1 + x5 + x7 + y8 \\
t8 &= x8 + y1 + y5 + y7 + y9 \\
t9 &= x1 + x5 + x7 + x9 + y2 + y6 + y10 \\
t10 &= x2 + x6 + x10 + y1 + y3 + y5 + y9 + y11 \\
t11 &= x1 + x3 + x5 + x9 + x11 + y4 + y12 \\
t12 &= x4 + x12 + y1 + y3 + y9 + y11 + y13 \\
t13 &= x1 + x3 + x9 + x11 + x13 + y2 + y10 + y14 \\
t14 &= x2 + x10 + x14 + y1 + y9 + y13 + y15 \\
t15 &= x1 + x9 + x13 + x15 + y16
\end{aligned} \tag{2}
$$

Encryption function

In this paper, a partial encryption algorithm for 3 bits is proposed. It begins by encrypting the least significant bits, then the next group goes through its position and so on, until it covers all positions by performing such shift 8 times. In Ref. (Espinosa, 2018) the equations (3) were used for full 8-bit encryption.

$$
\begin{aligned}
c1 &= t1 \oplus t9 \oplus t13 \oplus t15 \oplus \widehat{p1} \\
c2 &= t2 \oplus t10 \oplus t14 \oplus \widehat{p2} \\
c3 &= t3 \oplus t11 \oplus t15 \oplus \widehat{p1} \oplus \widehat{p3} \\
c4 &= t4 \oplus t12 \oplus \widehat{p4} \\
c5 &= t5 \oplus t13 \oplus \widehat{p3} \oplus \widehat{p5} \\
c6 &= t6 \oplus t14 \oplus \widehat{p2} \oplus \widehat{p6} \\
c7 &= t7 \oplus t15 \oplus \widehat{p1} \oplus \widehat{p3} \oplus \widehat{p5} \oplus \widehat{p7} \\
c8 &= t8 \oplus \widehat{p8}
\end{aligned} \tag{3}
$$

ISSN 2414-4924

Where ***c*** is encrypted text, ***t*** equals the secret key, and $\widehat{\boldsymbol{p}}$ is processed text.

Processing function

The processing function allows the calculation of a pseudorandom sequence through the backwards evolution in time of the cellular automaton. In Ref. (Urias, 1998) a pseudorandom number generator (PRNG) was used as a processing function, where the clear and random text blocks are taken as Boolean vectors. This processing and deprocessing function allows to change highly redundant values for others, with uniform distribution. The implementation of this generator is given by the following equations (4) and (5), based on ref. (Espinosa, 2018).

Processing

$$\begin{aligned}
\widehat{p1} &= p1 \oplus z2 \\
\widehat{p2} &= p2 \oplus z1 \oplus z3 \\
\widehat{p3} &= p1 \oplus p3 \oplus z4 \\
\widehat{p4} &= p4 \oplus z1 \oplus z3 \oplus z5 \\
\widehat{p5} &= p1 \oplus p3 \oplus p5 \oplus z2 \oplus z6 \\
\widehat{p6} &= p2 \oplus p6 \oplus z1 \oplus z5 \oplus z7 \\
\widehat{p7} &= p1 \oplus p5 \oplus p7 \oplus z8 \\
\widehat{p8} &= p8 \oplus z1 \oplus z5 \oplus z7 \oplus z9
\end{aligned} \tag{4}$$

Unprocessing

$$\begin{aligned}
p1 &= \widehat{p1} \oplus z2 \\
p2 &= \widehat{p2} \oplus z1 \oplus z3 \\
p3 &= \widehat{p1} \oplus \widehat{p3} \oplus z2 \oplus z4 \\
p4 &= \widehat{p4} \oplus z1 \oplus z3 \oplus z5 \\
p5 &= \widehat{p3} \oplus \widehat{p5} \oplus z2 \oplus z4 \oplus z6 \\
p6 &= \widehat{p2} \oplus \widehat{p6} \oplus z3 \oplus z5 \oplus z7 \\
p7 &= \widehat{p1} \oplus \widehat{p3} \oplus \widehat{p5} \oplus \widehat{p7} \oplus z4 \oplus z6 \oplus z8 \\
p8 &= \widehat{p8} \oplus z1 \oplus z5 \oplus z7 \oplus z9
\end{aligned} \tag{5}$$

Development

To perform the dynamic partial system, groups of 3 equations are made to encrypt the processed bits of $\widehat{\boldsymbol{p}}$. Table 1 shows the 8 encryption versions considered.

Version	Encrypted Bits
1	*c1 , c2, c3*
2	*c2 , c3, c4*
3	*c3 , c4, c5*
4	*c4 , c5, c6*
5	*c5 , c6, c7*
6	*c6 , c7, c8*
7	*c7 , c8, c1*
8	*c8 , c1, c2*

Table 1 Versions of partial encryption algorithms
Source: Prepared by the authors

Through this proposed algorithm, the user will be able to choose different versions of encryption mentioned in Table 1, in the order they want, due to its dynamic behavior. Therefore, the algorithm to encrypt an image consists of the following steps:

1. First, the image to be encrypted is selected.

Figure 3 Grayscale Lena image
Source: Prepared by the authors

2. The sequence of the encryption version taken from Table 1 of 8 combinations is chosen.

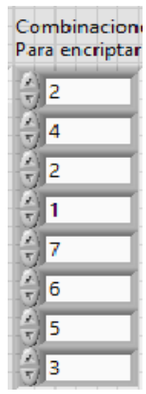

Figure 4 Key sequence for encryption
Source: Prepared by the authors

3. The pixel is entered as a block of clear text and we get *p*.
4. Then the pixel is processed with the vector *z* to obtain $\widehat{\boldsymbol{p}}$.
5. The *t* key is generated using the equations (2).
6. The 3 bits of the image are encrypted according to the encryption version in turn.
7. The encryption version is changed and repeated from step 2 to 6, until the entire image is encrypted.
8. The encrypted image is obtained.

ISSN 2414-4924

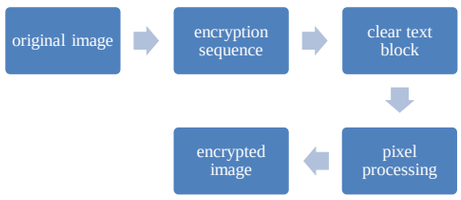

Figure 5 Steps for dynamic partial encryption
Source: Prepared by the authors

Results

To test the proposed encryption method, we considered the algorithm for several 512x512 grayscale images.

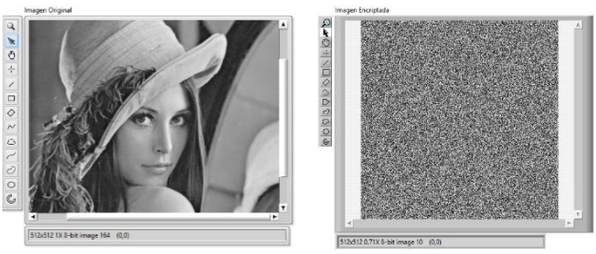

(a) (b)

Figure 6 (a) Original image of Lena. (b) Lena encrypted image using the proposed encryption
Source: Prepared by the authors

To measure the quality of the proposed encryption, several statistical tests were used, such as: histogram analysis and correlation coefficients (González, 2019), as well as cryptanalysis tests: Chosen-plaintext attack and bit replacement. The results are shown below:

Statistical Tests

Histograms

Histogram analysis shows how the pixels of an image are distributed, plotting the number of pixels according to the grayscale level. It consists of a test that measures the distribution of the pixels between the original and the encrypted image. In Fig. 7. the histogram of the original image is displayed, while in Fig. 8. the resulting histogram of the encrypted image is displayed. As we can see, the histograms of both images are different.

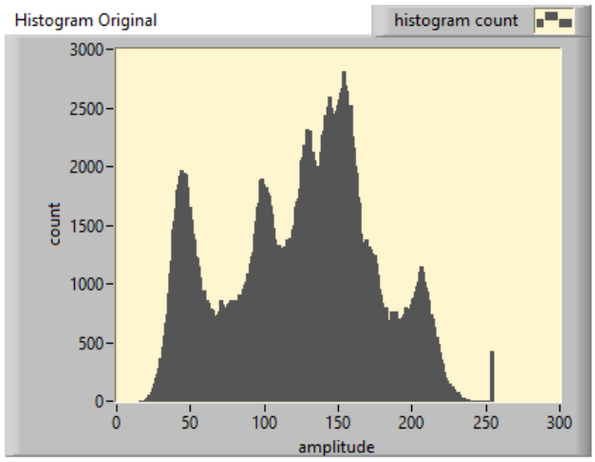

Figure 7 Histogram of the original image
Source: Prepared by the authors

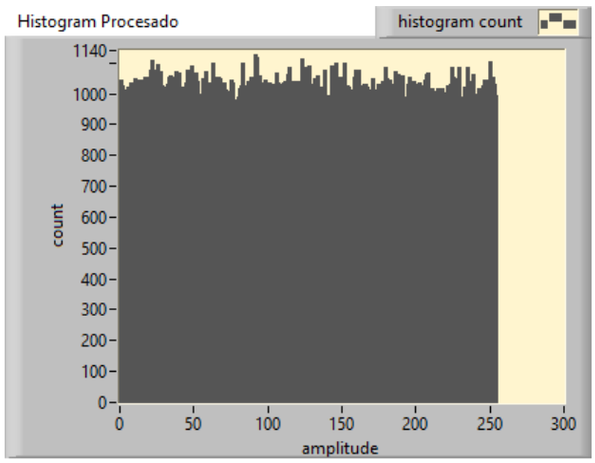

Figure 8 Histogram of the encrypted image
Source: Prepared by the authors

Correlation coefficients

In order to demonstrate that the encrypted image is different from the original image, we calculated the correlation coefficients between both images. If the calculated coefficient is close to 0 on both sides, it determines that there is no weak linear correlation, thus, the proposed system shows good performance. The results are shown in Table 2.

Image	Correlation
Lena	0.0001186

Table 2 Correlation coefficients of the encrypted image
Source: Prepared by the authors

Cryptanalysis Tests

Chosen plain-text attack

This test is intended for the attacker to reduce the security of the encryption system and reveal information.

ISSN 2414-4924

Attackers can choose some images arbitrarily (images where all pixels have the same value), and obtain the corresponding encrypted images, all under the same conditions of the type of encryption used. The tests performed are shown in Fig. 9.

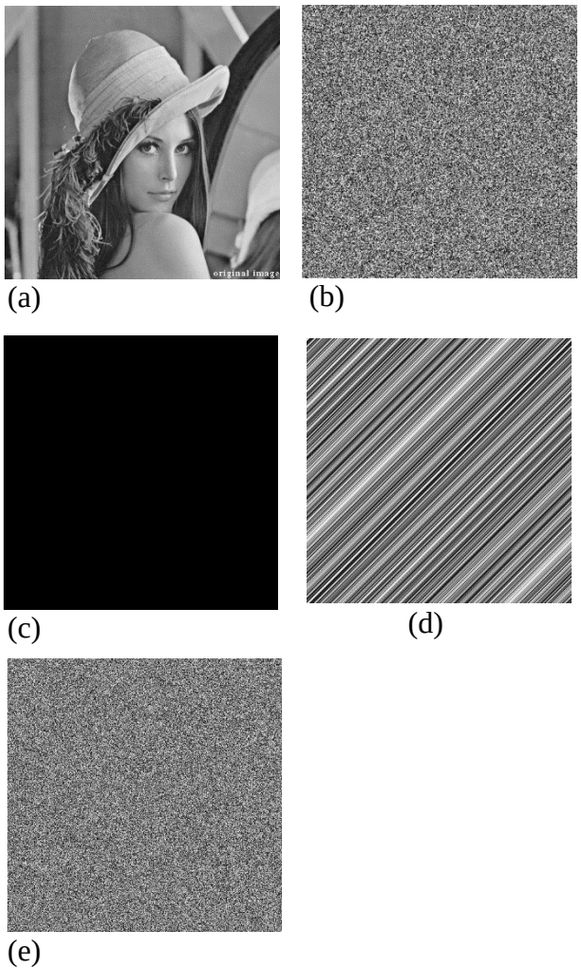

Figure 9 (a) Original image of Lena. (b) Encrypted image of (a). (c) Selected flat image. (d) Encrypted image of (c). (e) Image recovered
Source: Prepared by the authors

Replacement Attack

Assuming that the proposed encryption is secure, we carry out the attack known as a replacement attack, which consists on directly reconstructing the encrypted images. In this attack, the encrypted parts are replaced by artificial data that mimic the typical images [*IX*]. The encrypted bit plane is replaced by a constant 0, and the resulting decrease in the measured luminance is compensated by adding 64 to each pixel if only the most significant bit plane is encrypted. In Fig. 10. the resulting image can be seen, where no information is disclosed, denoting that the proposed system is safe.

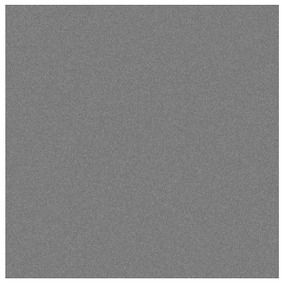

Figure 10 Image resulting from the replacement attack
Source: Prepared by the authors

Conclusions

In the present work, a dynamic partial encryption system for digital images was proposed, which was able to offer cryptographic security by using the synchronization of cellular automatons and rule 90 to better encrypt this information. Different statistical and cryptanalysis tests were carried out, with the success of the proposed algorithm. Therefore, this algorithm can be implemented in the encryption of important information.

References

Espinosa Olvera O. J. Análisis Estadístico de Cifrado Parcial, en imágenes digitales, UASLP, IICO, February 2018.

González Del Río Juan Daniel (2019). Diseño de trayectorias caóticas mediante el aumento de puntos de equilibrio en sistemas lineales por pedazos y su aplicación a la criptografía, (bachelor thesis). Universidad Autónoma de San Luis Potosí, CARAO, Salinas, SLP.

Lian, S. (2008). Multimedia content encryption: techniques and applications. Auerbach Publications.

Podesser, M., Schmidt, H. P., & Uhl, A. (2002, October). Selective bitplane encryption for secure transmission of image data in mobile environments. In CD-ROM Proceedings of the 5th IEEE Nordic Signal Processing Symposium (NORSIG 2002).

Ramirez Torres Marco Tulio, Application and implementation of an improved encryption system, (tesis de doctorado). Universidad Autónoma de San Luis Potosí, IICO, San Luis Potosí (2015).

Urias, J., Ugalde, E., Salazar, G.: Synchronization of cellular automaton pairs. Chaos: An Interdisciplinary Journal of Nonlinear Science, Vol. 8(4). AIP (1998) 814–818.

ISSN 2414-4924

Urias, J., Ugalde, E., Salazar, G.: A cryptosystem based on cellular automata. Chaos: An Interdisciplinary Journal of Nonlinear Science, Vol. 8(4). AIP (1998) 819–822.

Von Neuman, J.: Theory of Self-Reproducing Automata. Burks, A, W. University of Illinois Press (1966) 64-87.

Wolfram, S. Cellular automata and complexity: collected papres. CRC Press, (2018).:

ISSN 2414-4924

Article **ECORFAN Journal-Democratic Republic of Congo**
December 2019 Vol.5 No.9 17-29

Oscillation of a pendulum subject to a horizontal trajectory with different kinds of motion

Oscilación de un péndulo sujeto a una trayectoria horizontal con diferentes clases de movimiento

ESPINDOLA-HEREDIA, Rodolfo†*, DEL VALLE, Gabriela, MUCIÑO-CRUZ, Damián and HERNANDEZ-MORALES, Guadalupe

Universidad Autónoma Metropolitana-Unidad Azcapotzalco, División de Ciencias Básicas e Ingeniería, Dpto. Ciencias Básicas, área Física Atómica Molecular Aplicada, Laboratorio de Investigación en Dinámica Rotacional, Edificio G-103.

ID 1st Author: *Rodolfo, Espindola-Heredia* / **ORC ID**: 0000-0002-3641-5801, **CVU CONACYT ID**: 40866

ID 1st Coauthor: *Gabriela, Del Valle* / **ORC ID**: 0000-0003-4559-5792, **CVU CONACYT ID**: 1000607

ID 2nd Coauthor: *Damián, Muciño-Cruz* / **ORC ID**: 0000-0002-8710-9679, **CVU CONACYT ID**: 1000611

ID 3rd Coauthor: *Guadalupe, Hernandez-Morales* / **ORC ID**: 0000-0002-6793-273X, **CVU CONACYT ID**: 74002

DOI: 10.35429/EJDRC.2019.9.5.17.29 Received July 28, 2019; Accepted December 20, 2019

Abstract

In the children's movie *The Incredibles* there is a scene where Mr Incredible faces Bomb Voyage, while Incredi Boy wants to help Mr Incredible, Incredi Boy flies with Mr Incredible, who holds on to the hero's cloak, affecting Incredi Boy's flight plan. To understand how an oscillatory movement affects non-oscillatory movement, an experimental prototype was constructed with a particle of mass m, attached to a rigid rod and without mass of length l, to a swivel of negligible mass, which was subject to a mass *M*. The swivel always remained on a horizontal plane, allowing the oscillatory movement of mass m. Experimental results were obtained by means of wireless sensors which recorded the spatial coordinates of the mass m. Using Lagrangian mechanics we obtained the equations of motion and expressed the possible first integrals of movement, when the movement of the mass *M* was: linear uniform (ULM), uniformly accelerated, (UAM), uniform circular (UCM), accelerated circular (ACM) and forced circular (FCM). The dynamics were analyzed, the equations of movement obtained, they were solved numerically, and the experimental results were compared to theoretical and numerical results.

Mechanics, Simulation, No-inertial-Movement

Resumen

En una película infantil hay una escena, Mr Increíble enfrenta a Bomb Voyage, el niño Incredi Boy quiere ayudar a Mr Increible, Incredi Boy vuela con Mr increíble, quien se sostiene de la capa del héroe, afectando el plan de vuelo de Incredi Boy. Para entender cómo afecta un movimiento oscilatorio al movimiento no oscilatorio, se construye un prototipo experimental con una partícula de masa m, unida a una varilla rígida y sin masa de longitud l, a una rótula de masa despreciable, la cual está sujeta a una masa M. La rótula permanece en todo instante sobre un plano horizontal y permite el movimiento oscilatorio de la masa m. Se obtienen resultados experimentales que son recabados por medio de sensores inalámbricos que permiten la obtención de coordenadas espaciales de la masa m. Usando mecánica Lagrangiana se obtienen las ecuaciones de movimiento, expresamos las posibles integrales primeras de movimiento, cuando el movimiento de la masa M es: rectilíneo uniforme, (MRU), uniformemente acelerado, (MRUA) circular uniforme (MCU), circular acelerado (MCA) y circular forzado (MCF). Se analiza la dinámica, se obtienen las ecuaciones de movimiento, se resuelven numéricamente, y se contrastan los resultados experimentales con resultados teóricos y numéricos.

Mecánica, Simulación, Sistema-no-inercial

Citation: ESPINDOLA-HEREDIA, Rodolfo, DEL VALLE, Gabriela, MUCIÑO-CRUZ, Damián and HERNANDEZ-MORALES, Guadalupe. Oscillation of a pendulum subject to a horizontal trajectory with different kinds of motion. ECORFAN Journal-Democratic Republic of Congo. 2019, 5-9: 17-29

* Correspondence to Author (email: roeshe@azc.uam.mx)
† Researcher contributing first author.

Introduction

In the children's movie *The Incredibles I*, Mr. Incredible when facing one of the villains, the famous Bomb Voyage, is helped by his biggest fan, a boy named Buddy Pine, who would later become his archenemy. Mr. Incredible clarifies to the boy that he works alone and does not want to deal with Incrediboy (Buddy Pine), Incrediboy insists to be part of the incredible celebrities who help the world against the wicked and considers that searching for help can be a way to start participating with Mr. Incredible.

On his way out, the evil Bomb Voyage places one of his bombs on the boy's cape, Mr. Incredible upon realizing it, releases the villain and runs to rescue the child. The boy is equipped with shoes that allow him to fly, he starts his flight just when Mr. Incredible grabs his cape, the child's flight then becomes unstable and erratic due to the oscillation of the body of the super Hero with the boy's cape and, of course, to Mr. Incredible's own weight.

We take this fact to study the dynamics of a movement like that described in the movie. Our goal is to understand how a three-dimensional (3D) movement for a given object is disturbed by the oscillation of a second object subject to the first. This kind of movements occur in real life and this research may have applications for practical cases, for example: when a helicopter by means of a cable, carries a certain mass, like a sculpture, or moves granular material to put out a fire, etc.

Carrying out the investigation for a 3D case of a flying object is our final goal; for this, we show results for certain cases of the study system, which will allow us to subsequently establish the general case in 3D.

The system (see Figure 1) is formed by a particle of mass *m*, which is attached through a rigid rod of length *l* without mass to a ball of negligible mass, which is subject to another object of mass *M*; the swivel at all times remains on a horizontal plane and allows the oscillatory movement of the particle of mass *m*. The movement of the mass particle *M* obeys the following cases: uniform linear motion (ULM), uniformly accelerated linear motion (UALM), uniform circular motion (UCM), uniformly accelerated circular motion (UACM).

The dynamic properties of the system are studied through Lagrangian dynamics, the energies are obtained to subsequently obtain the equations of motion through the Euler-Lagrange equations and thus study the coupling between the linear and angular variables.

Likewise, the study is carried out from an experimental device in accordance with the system described above, results are obtained on the acceleration of mass *M* with the help of wireless communication by means of sensors, which are provided with accelerometer, compass and gyroscope, allowing the obtention of linear and angular acceleration values. Numerical results of the motion equations are also obtained by solving the system of differential motion equations for each case. We discuss their tendency to chaos and contrast the experimental results with the numerical ones.

Theory

a) Uniform Linear Motions and Uniformly Accelerated Linear Motion

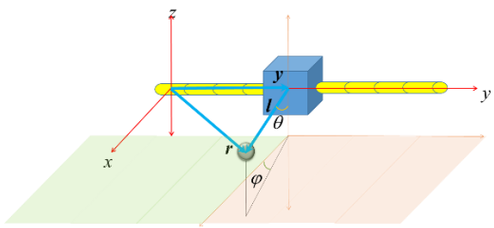

Figure 1 Description of the study system

We first consider the case when the mass *M* moves in a straight line in the direction of the *y*-axis, the inertial reference system selected to study both the movement of the mass *M* and the pendulum of mass *m* and length *l* is shown in Figure 1 and it is determined by the *x*, *y*, *z* axes. Note that the position vectors: $\vec{r}$ that locates the mass *m*, $\vec{y}$ that locates the mass *M* and $\vec{l}$ that locates the mass *m*, from the center of mass of *M*, form a triangular polygon, which allows the three vectors to be related:

$$\vec{r} = \vec{y} + \vec{l} \tag{1}$$

The $\vec{y}$ and $\vec{r}$ vectors are given by the following two equations:

$$\vec{y} = y\,\hat{j} \tag{2}$$

ISSN 2414-4924

$$\vec{r} = l\ \cos\varphi \sin\theta\ \hat{\imath} + l \sin\varphi\ \sin\theta\ \hat{\jmath} - l \sin\theta\ \hat{k} \quad (3)$$

As the coordinate of interest is $\vec{r}$, in order to construct the kinetic energy of the pendular mass: $K = m\,\dot{r}^2/2$, in the case of the pendulum, it is necessary to obtain $\vec{r}$ ˙, with (1-3) and then taking the internal product $\dot{r}^2 = \dot{\vec{r}} \cdot \dot{\vec{r}}$ to establish the kinetic energy of the mass *m*:

$$K_m = \frac{1}{2}m\left(l^2 \sin\theta^2\,\dot{\theta}^2 + \left(-l \sin\theta \sin\varphi\,\dot{\theta} + l\cos\theta\cos\varphi\,\dot{\varphi}\right)^2 + \left(\dot{y} + l\cos\theta\sin\varphi\ \dot{\theta} + l\cos\varphi\sin\theta\ \dot{\varphi}\right)^2\right) \quad (4)$$

It is possible to observe that this kinetic energy depends on the variables: $(\dot{y}, \theta, \dot{\theta}, \varphi, \dot{\varphi})$. The kinetic energy of the mass object *M* will be given by:

$$K_M = \frac{1}{2}M\dot{y}^2 \quad (5)$$

Where $\dot{y}$ is the velocity of mass *M*. Because it travels on an equipotential gravitational surface, the change in its gravitational potential energy is zero and the contribution to gravitational potential energy is due only to the pendular mass, which is:

$$U = -m\ g\ l\ \cos\theta \quad (6)$$

The Lagrangian function (Herber Goldstein, 2000) of the system is obtained in the standard way: *L* = *K*-*U*. Through the Euler-Lagrange equation: $\frac{d}{dt}\frac{\partial L}{\partial \dot{q}} - \frac{\partial L}{\partial q} = 0$, the three equations of motion are obtained, for the time-dependent dynamic variables: $\theta(t), \varphi(t), y(t)$ as follows:

$$\ddot{\theta} = \frac{2g\sin\theta + l\sin 2\theta\dot{\theta}^2 + 2l\sin 2\varphi\ \dot{\theta}\dot{\varphi} + 2\cos\theta\sin\varphi\ \ddot{y}}{-2l + l\cos 2\theta + l\cos 2\varphi} \quad (7)$$

$$\ddot{\varphi} = -\frac{\sec\varphi\sin\theta\,\ddot{y}}{l} + \tan\varphi\,\dot{\theta}^2 + \tan\varphi\,\dot{\varphi}^2 \quad (8)$$

$$\ddot{y} = \frac{lm\sin\theta\sin\varphi\dot{\theta}^2}{m+M} - \frac{2lm\cos\theta\cos\varphi\dot{\theta}\dot{\varphi}}{m+M} - \frac{lm\sin\theta\sin\varphi\ddot{\varphi}^2}{m+M} - \frac{lm\cos\theta\sin\varphi\ \ddot{\theta}}{m+M} - \frac{lm\cos\varphi\sin\theta\ddot{\varphi}}{m+M} \quad (9)$$

It is possible to continue along this path, so it is necessary that the set of three ordinary differential equations of the second order be reduced.

It is observed that the dynamic variables $\ddot{\theta}(t), \ddot{\varphi}(t), \ddot{y}(t)$ are coupled to reduce the system of equations, substitute (9) in equations (7) and (8) to obtain a set of two differential equations with two variables; with this, the information of the linear variable *y* is lost, which can be known from the results for θ and φ.

However, it is possible to obtain more information because in this Lagrangian the *y* coordinate is a cyclic coordinate, since there is no dependence on it in the Lagrangian and only depend on $\dot{y}$, that is:

$$\frac{\partial L}{\partial \dot{y}} = p_y = M\dot{y} \quad (10)$$

Where p_y is the linear momentum of mass *M*, combining the results, we have:

$$\dot{y} = -l(\cos\theta\sin\varphi\dot{\theta} + \cos\varphi\sin\theta\dot{\varphi}) \quad (11)$$

Equation (11) is integrated to obtain the following result:

$$y = \int dy = -l\int\left(\cos\theta\sin\varphi d\theta\right) - -l\int\left(\cos\varphi\sin\theta d\varphi\right) = = -2l\sin\theta\sin\varphi \quad (12)$$

This result is interesting because although it is true it is negative, the function *sin(x)* is sometimes positive and sometimes negative; it is also assumed that although the variables θ and φ are coupled, we do not know if they are found in phase or not, so that result indicates that certainly the car sometimes moves forward and sometimes backwards. With these results, we prepared the simulation to analyze the dynamic states of the system.

b) Circular Motion

c)

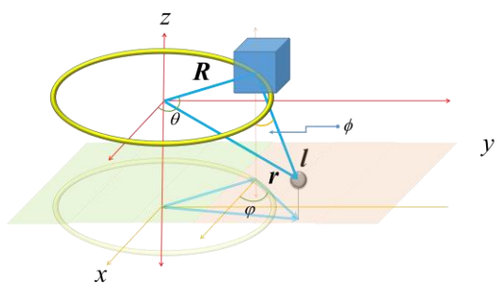

Figure 2 Description of the study system in uniform circular motion

For this case, we considered Figure 2 and observed that the triangular polygon is formed by the vectors $\vec{R}, \vec{l}\ and\ \vec{r}$. The way in which the three vectors are related is given by:

$$\vec{r} = \vec{R} + \vec{l} \tag{13}$$

In rectangular coordinates the vector $\vec{R}$ is written as:

$$\vec{R} = R\ \cos\theta\ \hat{\imath} + R\ \sin\theta\ \hat{\jmath} \tag{14}$$

Where R is the radius of the circumference where the object of mass M will move and θ is the azimuth angle. The vector $\vec{l}$ locates the pendular mass from the center of mass of the object of mass M, the pendular mass can move in three dimensions, so that the vector $\vec{l}$ is written based on the variables of Figure 2 as:

$$\vec{l} = l\ \sin\phi\cos\varphi\ \hat{\imath} + l\ \sin\phi\sin\varphi\ \hat{\jmath} - l\cos\phi\ \hat{k} \tag{15}$$

with (10) (11) and (12) $\vec{r}$ is established as,

$$\vec{r} = (R\cos\theta + l\ \sin\phi\cos\varphi)\ \hat{\imath} + (R\ \sin\theta + l\ \sin\phi\sin\varphi)\ \hat{\jmath} - l\cos\phi\ \hat{k} \tag{16}$$

by proceeding in the same way as for the linear case we have:

$$K_m = \frac{1}{2}m\ (R^2\dot{\theta}^2 + 2lR\dot{\theta}\left(-\cos\phi\ \sin(\theta - \varphi)\dot{\phi} + \cos(\theta-\varphi)\sin\phi\,\dot{\varphi}\right) + l^2(\dot{\phi}^2 + \sin\phi^2\,\dot{\varphi}^2)) \tag{17}$$

and K_M is obtained with:

$$K_M = \frac{1}{2}M\ R^2\dot{\theta}^2 \tag{18}$$

The potential energy is only gravitational and is corresponding to the pendulum as follows:

$$U_{g_m} = -m\ l\ g\cos\phi \tag{19}$$

Of course, once the Lagrangian is obtained, we proceeded in the same way: through the equation of Euler Lagrange the equations of movement are obtained for the three dynamic variables:

$$\ddot{\theta} = -\frac{lm\sin\phi\sin(\theta-\varphi)\dot{\phi}^2}{(m+M)R} - \frac{2lm\cos\phi\cos(\theta-\varphi)\dot{\phi}\dot{\varphi}}{(m+M)R} - \frac{lm\sin\phi\sin(\theta-\varphi)\dot{\varphi}^2}{(m+M)R} + \frac{lm\cos\phi\sin(\theta-\varphi)\ddot{\phi}}{(m+M)R} - \frac{lm\cos(\theta-\varphi)\sin\phi\ddot{\varphi}}{(m+M)R} \tag{20}$$

$$\ddot{\phi} = -\frac{g\sin\phi}{l} + \frac{R\cos\phi\cos(\theta-\varphi)\,\dot{\theta}^2}{l} + \cos\phi\sin\phi\dot{\varphi}^2 + \frac{R\cos\phi\sin(\theta-\varphi)\ddot{\theta}}{l} \tag{21}$$

$$\ddot{\varphi} = \frac{R\csc\phi\sin(\theta-\varphi)\dot{\theta}^2}{l} - 2\cot\phi\,\dot{\phi}\dot{\varphi} - \frac{R\cos(\theta-\varphi)\csc\phi\ddot{\theta}}{l} \tag{22}$$

In this set of three second-order ordinary differential equations, the dynamic variables are also coupled. To solve the system, it is necessary that (21) and (22) are substituted in (20), to obtain an equation for $\ddot{\theta}$ which only depends on the generalized coordinates $\theta, \phi, \varphi, \dot{\theta}, \dot{\phi}\ and\ \dot{\varphi}$. Then, once having that result for (20), it is also substituted in both (21) and (22) to obtain three equations dependent only on the generalized coordinates, and solve by numerical methods, the set of differential equations. Unlike the previous case, there is no cyclical coordinate here, which indicates that there is no conservation of any associated moment or amount of movement.

Simulation

In order to carry out the simulation of the described systems, a change of variable is usually suggested to reduce the system to a first order, the results obtained by the simulation correspond to the values q and $\dot{q}$ since $\ddot{q}$is known, which is described by equations (7-9) for the case of linear motion and (20-22) for circular motion.

The numerical method used to solve the differential equations is the Runge-Kutta method of order 4 (*RK4*). The choice of the method is essentially because it is the most standardized, we have it programmed and it has served for the numerical solution of other problems and dynamic systems that we have studied.

There are currently several computer programs that intrinsically have a variety of solution methods programmed for differential equations; however, we chose to develop our own code, because these programs represent a black box for the user.

ISSN 2414-4924

This method is explained and applied for simple systems in books of numerical methods (Timothy Sauer, 2013), as well as in books of differential equations (W. E Boyce, 2004). The error due to the use of the method is of the order of the step size, which we denote by δh raised to the 4, that is, $\varepsilon rr = \Delta h^4$. The step size is defined as the partition of the integration interval $\delta h = (b-a)/n$, where b is the upper limit of the interval, a is the lower limit, n the number of parts into which the interval is divided, which in fact corresponds to the number of iterations that will have to be done to cover the entire proposed integration interval (b-a). For case a) we have δh = 0.0011 and for case b) δh = 0.0019, throwing an error $\varepsilon rr = 1.4 \times 10^{-12}$, $\varepsilon rr = 1.4 \times 10^{-11}$, respectively.

UALM simulation details

Table 1 contains the values of the properties used in the simulation: g is the value of the acceleration of gravity, equal to the value reported for Mexico City. The upper limit of the simulation was taken as 1.1, because when exceeding this value, it has problems with the values obtained from the calculation, this is because in the equations to integrate, there are trigonometric functions such as tangent and reactive, which around this value is probable that the system approaches some asymptote, so the function is undetermined.

The length of the pendulum is denoted by *l*, *m* is the pendular mass, and *M* is the mass of the car. The rest are initial conditions (IC) to solve the equations. *N* is the number of times we repeated the numerical experiment; each repetition of the experiment was performed with new ICs. In order to observe the changes produced by the new ICs, it was decided to only make small changes systematically, for this purpose changes were proposed only in the variables related to speed:

$$\begin{aligned} \dot{y_0} &= \dot{y_0} + 0.09 \\ \dot{\theta_0} &= \dot{\theta_0} + 0.09 \\ \dot{\varphi_0} &= \dot{\varphi_0} + 0.10 \end{aligned} \tag{23}$$

UALM simulation					
prop	***value***	***unit***	***prop***	***value***	***unit***
g	9.780	m/s^2	$\boldsymbol{y_0}$	0.1	m
a	0.000	adim	$\boldsymbol{\dot{y}_0}$	3.1	m/s
b	1.100	adim	$\boldsymbol{\theta_0}$	1.1	grad
n	1000	adim	$\boldsymbol{\dot{\theta}_0}$	5.3	rad/s
l	0.450	m	$\boldsymbol{\phi_0}$	1.5	grad
m	0.270	Kg	$\boldsymbol{\dot{\phi}_0}$	5.1	rad/s
M	0.332	kg	**N**	21	adim

Table 1 Initial property and condition values

UACM Simulation Details

In the case of the UACM simulation, the gravity acceleration value was taken in the same way as in the previous case, which is why it does not appear in Table 2.

UACM simulation					
prop	***value***	***unit***	***Prop***	***value***	***unit***
a	0.000	m/s^2	$\boldsymbol{\theta_0}$	1.1	m
b	1.100	adim	$\boldsymbol{\dot{\theta}_0}$	3.3	m/s
n	7000	adim	$\boldsymbol{\phi_0}$	1.1	grad
R	0.450	M	$\boldsymbol{\dot{\phi}_0}$	6.3	rad/s
l	0.350	M	$\boldsymbol{\varphi_0}$	1.1	grad
m	0.270	Kg	$\boldsymbol{\dot{\varphi}_0}$	10.1	rad/s
M	0.332	Kg	**N**	25	adim

Table 2 Initial property and condition values

Table 2 shows the values of the parameters used in the UACM simulation, as well as the required ICs, to obtain their solution. The parameter R appears, which represents the radius of the circle on which the car rotates. The ICs are for the angles, being θ the polar angle, ϕ the zenith angle, and φ the azimuth angle. Likewise, the ICs were changed for 25 numerical experiments, the following rules being in this case:

$$\begin{aligned} \dot{\theta_0} &= \dot{\theta_0} + 0.09 \\ \dot{\phi_0} &= \dot{\phi_0} + 0.10 \\ \dot{\varphi_0} &= \dot{\varphi_0} + 0.10 \end{aligned} \tag{24}$$

Experimental development

The experiment was carried out using a low-friction car PASCO (ME-1240) and two rails were implemented. At the beginning, two rails that rest on two rigid rods were used, each wheel of the low friction car moves over each one, a "ball joint" (swivel) was implemented so that the pendulum moved freely, the pendular mass is a *Naylamid* sphere.

ISSN 2414-4924

To attach the pendulum to the low-friction car, three parts were designed in Autodesk Inventor: one that serves as a special base to attach the swivel to the carriage, another to attach it to the pendulum rod and another to attach the rod to the pendulum mass. These pieces were 3D printed, an Anet A8 printer was used with Utimaker Cura 3.2.1.

Figure 3 Experimental device for uniform linear motion

Likewise, special bases were designed to mount the rails on horizontal rods supported to a universal support. Through a video shot, the experiment was recorded for the two cases presented a) linear motion and b) circular motion, with a radius of curvature R = 1.5 m. To follow the trajectory of the mobiles: car and pendulum, Traker Video Analysis and Modeling Tool were used, which allowed to collect the data of some of the studied properties, simultaneously data of the displacement of the low-friction car were collected by means of sensors with wireless "bluetooth" using as interface a cell phone in which the *SPARKvue* application was installed.

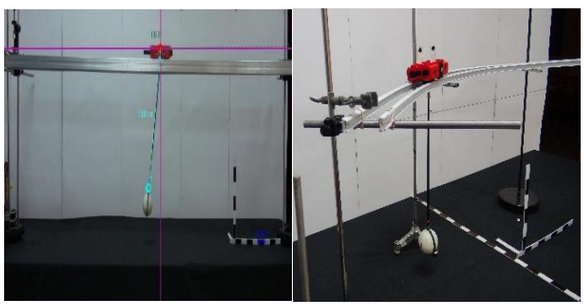

Figure 4 Experimental devices for both motions: uniform linear motion and uniform circular motion

To ensure that the initial car speed is the same in each video shot, a trigger was applied to the low-friction car (a piston activated by pressing a pivot on the top of the car, providing a boost, in this way it was also guaranteed that said impulse was of similar magnitude in each repetition of the experiment).

While the trigger was activated, the pendulum was placed at a certain angle, so that just at the moment when the car started its movement with a certain initial speed, the pendulum also began its wave motion.

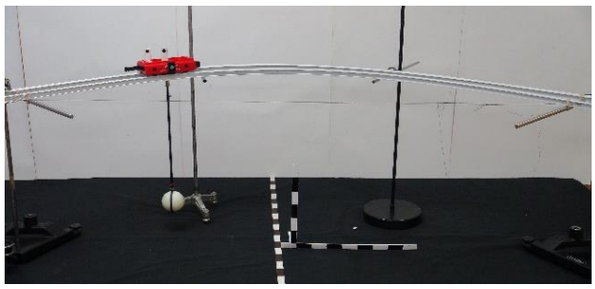

Figure 5 Experimental device for uniform circular motion

It is important to note that the video shots only allow us to analyze two dimensions, to monitor the movement of the pendulum in three dimensions requires preparing the scene much better and having more cameras and some other electronic devices to properly and correctly measure the dynamic variables of interest.

Numerical Results

UALM

The results obtained by simulation are several, because for each trial we get: time, position, velocity and acceleration of the object of mass M, as well as angular position, velocity and acceleration for the pendular mass m, given that the value of the pendulum length is known, it is possible to obtain the rectangular positions of the pendular mass m.

The phase diagrams show the behavior of the dynamic variables, these are of interest because the temporal parameter is eliminated and allow the observation of the existing changes between position and speed for each dynamic variable. Graph 1 shows the phase diagram for the y coordinate, the solution for y and $\dot{y}$, are given by (11-12), they certainly do not represent the numerical solution of the differential equation for y, but it is known from the numerical solutions for the angular coordinates θ and φ. In this graph, it is observed that the trajectory in the phase plane does not represent a closed curve, the change of ICs is also appreciated, by the different colors plotted, which shows the different trajectories that are quite similar to each other.

ISSN 2414-4924

It is not observed that the y variable is sensitive to the change in ICs.

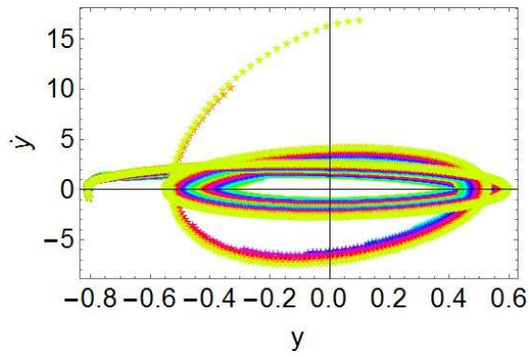

Graph 1 Phase diagram for coordinate y

Graph 2 shows the phase diagram for the angular coordinate θ. In this diagram the result each trial within the simulation is well-defined, this result corresponds to the numerical solution of equations (7). Again, it is observed that all curves describe a similar shape. However, changes in ICs result in separate curves, enlarged or contracted, which shows signs that the θ variable is chaotic.

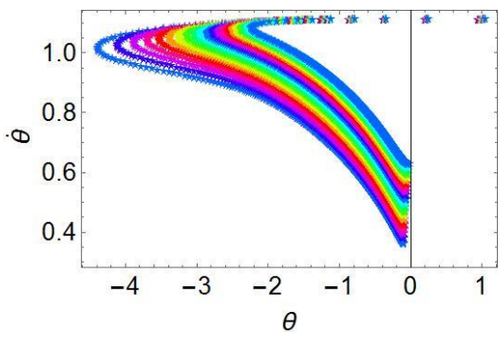

Graph 2 Phase diagram for coordinate θ

Graph 3 presents the phase diagram corresponding to the angular variable φ. Of the three phase diagrams, this has the least structure, since the behavior between the variables (φ vs. $\dot{\varphi}$) seems to be approximately logarithmic, the sensitivity to the changes of ICs shows only a shift in the curve.

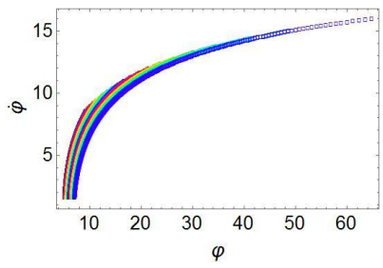

Graph 3 Phase diagram for coordinate φ

The result corresponding to the acceleration behavior in the direction y and the direction of movement of the mass object M proved to be relevant.

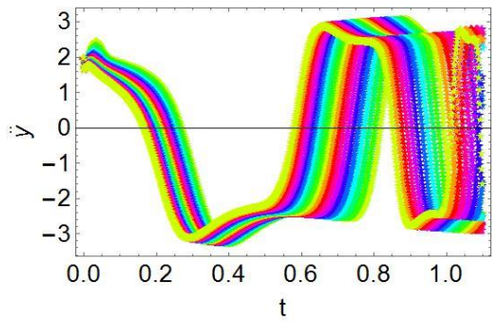

Graph 4 Result for acceleration in direction y: $(t\ vs.\ \ddot{y})$

Graph 4 shows the result for the 21 simulations performed. Acceleration is presented as a function of time, it exhibits greater sensitivity to changes in ICs; it is observed that the more the system moves from the origin coordinates, there is more variation between the trajectories, so there are more significant changes between each trial, which suggests that the system turns out to be chaotic. In this paper, no parameters related to the chaos of the system were measured, however, Graph 4, together with Graphs (2-3) motivates the possibility of doing so and directing attention in this direction. Another situation that can be seen in Graph 4 is that for some time intervals, the acceleration is negative, for others it is positive. The plot of the graph seems to tend approximately to an oscillatory movement with a certain frequency. Given the impossibility of measuring beyond the proposed values, it is not possible to observe this tendency with greater clarity, however, if it was possible to observe experimentally, the object of mass M sometimes moves forward and sometimes backwards, showing a behavior similar to that in Graph 4.

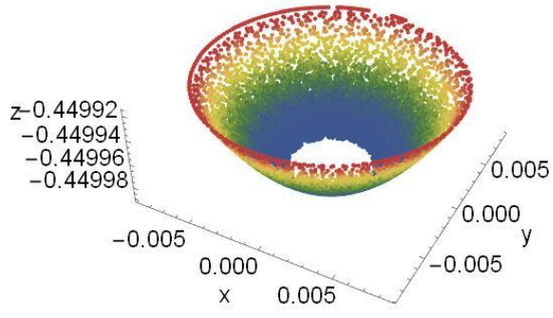

Graph 5 Result for the position of the pendular mass, in rectangular coordinates, from a fixed observer on object M.

Given the angular values obtained and the pendulum length, it is possible to obtain the position (*x*, *y*, *z*) of the pendular mass.

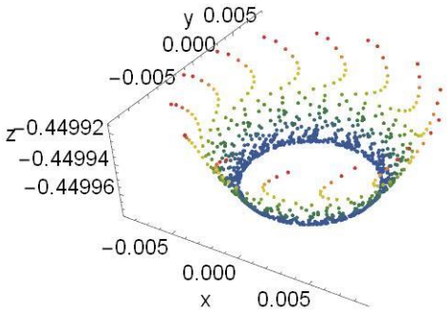

Graph 6 Result for the position of the pendular mass, in rectangular coordinates, for iteration 20. From a fixed observer on object *M*.

Graph 5 shows the trajectories for each of the 21 simulations performed, the result is that the positions of the pendular mass are located on the internal surface of a hemisphere of radius *l*, the gap that is observed at the bottom of the hemisphere result from the fact that the ICs do not start from zero. However, for any performed iteration, the pendulum will always be at a point on the surface of this hemisphere. The result shown in Graph 6 shows the iteration corresponding to trial number 20, presenting greater clarity in this regard.

It is necessary to note that what is shown in Graphs 5 and 6 is the observation of the movement of the pendulum from an observer who is on the object of mass *M*. As we have previously mentioned, object *M* moves with variable acceleration, therefore, this reference system corresponds to a non-inertial reference system. To have a result whose observation is from an inertial reference system, the pendulum's displacement must be measured from the fixed origin outside the object *M*, that is, the inertial reference zero, which is fixed to the left of the objects (see figure 1).

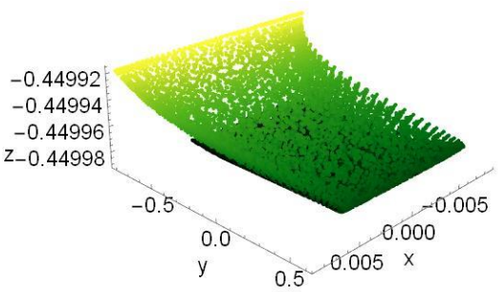

Graph 7 Result for the position of the pendular mass, in rectangular coordinates. From a fixed observer at the origin of coordinates

The observation from this inertial reference system is shown in figure 7.

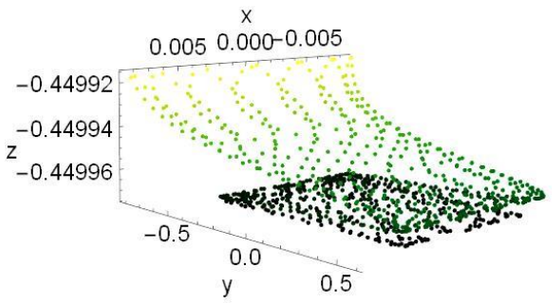

Graph 8 Result for the position of the pendular mass, in rectangular coordinates. From a fixed observer at the origin of coordinates

And the trajectory corresponding to trial 20 is shown in Graph 11, in both Graphs (7 and 8) the behavior of the coordinate *y* can be observed, which shows the effect of the oscillatory movement in the direction in which the object of mass *M* moves, displaying the behavior of a bending surface. These graphs have been presented as Graphs (5 and 6) exhibit the behavior of a spherical pendulum, which corresponds to the description of an observer looking at the fixed pendulum in *M*. However, a fixed observer in the inertial reference system *O* will see what is shown in Graphs (7 and 8).

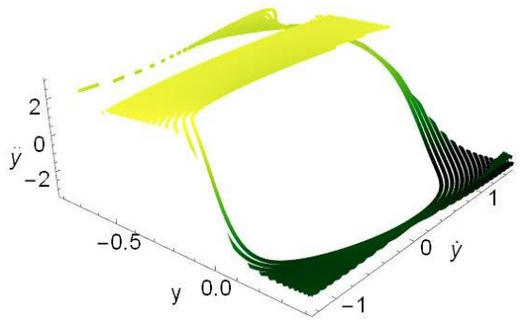

Graph 9 Coordinate *y* behavior, the relationship between position, speed and acceleration is shown

Once the results are obtained for all the variables, it is possible to review the behavior of the three coordinates simultaneously, this behavior is presented for the variables *y* and φ in Graphs (9 and 10).

ISSN 2414-4924

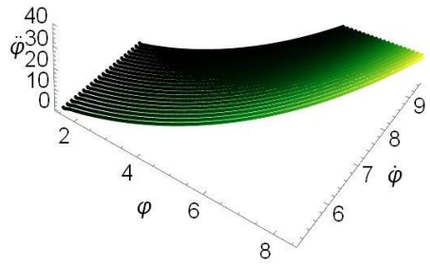

Graph 10 Behavior of the angular coordinate φ, the relationship between position, velocity and angular acceleration is shown. The behavior of the angular coordinate φ is quite stable, it presents only a small slope.

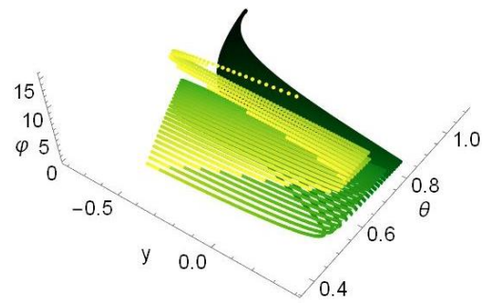

Graph 11 Behavior between both linear and angular positions. It can be observed a behavior that essentially has the same origin, but which, depending on the CIs, concludes at another point, that is, it shows a chaotic behavior mainly for the coordinate θ.

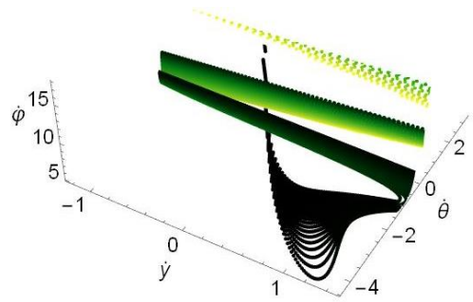

Graph 12 Behavior for linear and angular speeds. It is observed again that the graphs have a common origin, however the greatest change is provided by the θ. coordinate.

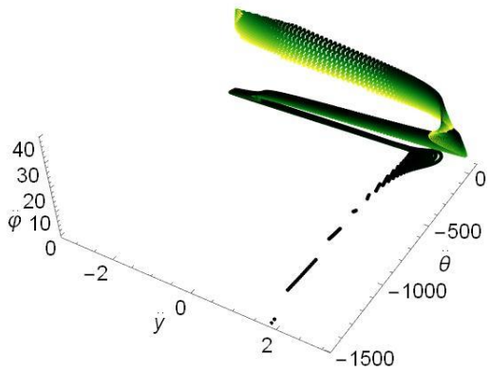

Graph 13 Acceleration behavior, a clear tendency to chaos in the acceleration behavior is observed.

Graphs (11-13) show the coupling behavior of the dynamic variables of the block-pendulum system and provide information on the effect of the linear movement of the mass block *M* by effect of or as a consequence of an oscillatory movement of the mass pendular *m*.

UACM

The numerical results for the case of circular motion allow us to obtain results on the dynamic variables θ, ϕ and φ, and on their temporal derivatives with which the phase diagrams can be constructed, as well as to observe the temporal evolution of each variable. Graph 14 presents the phase plane of the polar angular variable θ, which is the car's direction. A simple comparison between Graphs 1 and 14, allows us to observe that the behavior is different, due to the trajectories that the movement associated with the object of mass *M* follows.

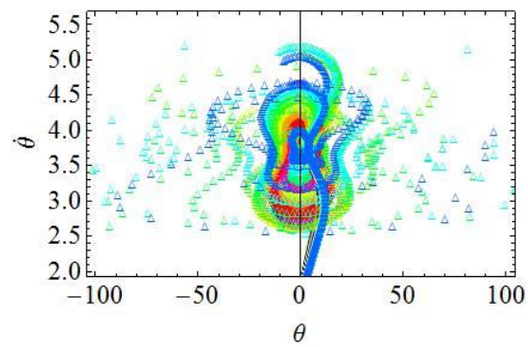

Graph 14 Phase plane for coordinate θ

However, in both cases the curves are open, it is also observed that for both cases the paths of the same trial cross more than once.

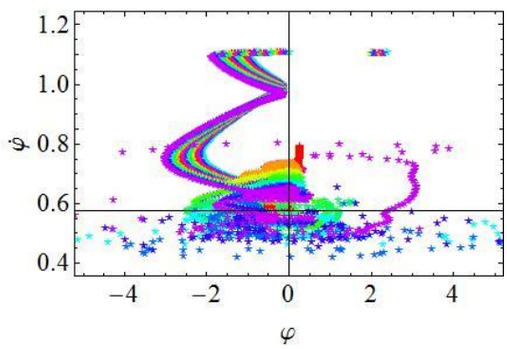

Graph 15 Phase diagram for the angular variable □

A much more chaotic result is appreciated for the UACM than for the UALM.

ISSN 2414-4924

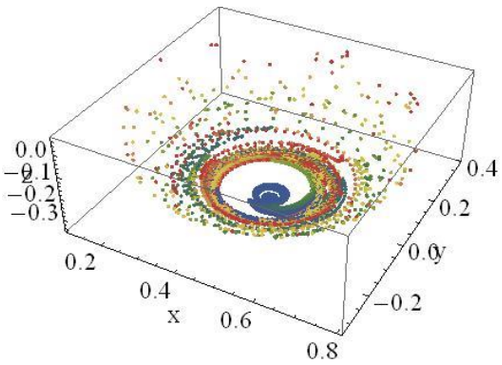

Graph 16 Space trajectories for the behavior of pendular mass in uniformly accelerated circular motion

Graph 15 shows the phase diagram for the azimuth angle φ, a comparison between Graphs 2 and 15 shows that in the case of the UACM, the azimuth coordinate is more chaotic. Similarly, it is possible to obtain the *x, y* and *z* coordinates of the pendular mass *m*, shown in Graph 16, where the spatial trajectory is observed for the 21 simulations performed for this case. The comparison between Graphs 5, 16 and 7, show a different behavior, a tendency to chaos. The movement of the pendular mass is erratic, even though at the beginning the internal structure of the trajectories presents a systematic and similar behavior to that of a spiral.

A two-dimensional view is presented in Graph 17. Different tests were made proposing various changes for the ICs; it was observed that the change for the angular velocity $\dot{\theta}$ presents an offset of the center of the circle for the initial spiral paths, the end values for each trajectory are very scattered, so the behavior shown by the pendular mass also tells us that in the circular motion of the object of mass *M*, its behavior is erratic.

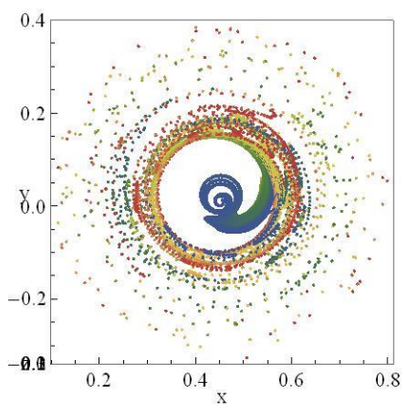

Graph 17 Spatial trajectories for the behavior of the pendular mass in the uniformly accelerated circular motion in two dimensions, corresponding to the coordinates (x, y).

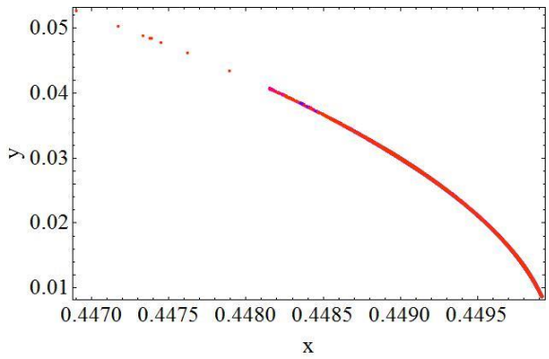

Graph 17 Spatial trajectories for the behavior of the pendular mass in the uniformly accelerated circular motion in two dimensions, corresponding to the coordinates (x, y)

Finally, Graph 18 shows the result for the trajectory of the object of mass *M*. Since the entire interval was not integrated, the trajectory shows only one segment; the total of the 21 results of the simulations fall on the same curve, which was expected.

Experimental Results

UALM

The experimental results obtained allow us to make purely qualitative comparisons. In order to obtain precise results to quantitatively contrast with the numerical results, we are solving the experimental inconveniences.

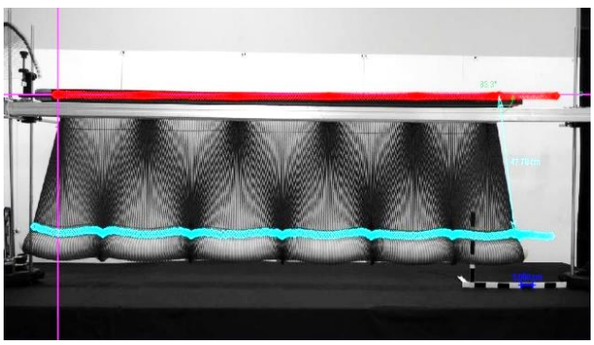

Figure 6 Space trajectories for pendular mass behavior in accelerated linear motion

Figure 6 shows a frame of the analysis by means of *Tracker*, the red curve corresponds to the tracking done to the object of mass *M*, while the blue curve represents the monitoring of the pendular mass *m*; in the same frame the movement of the rod is recorded. The effect of the pendulum is observed when moving inside the hemisphere, as indicated by Graphs (5-6).

ISSN 2414-4924

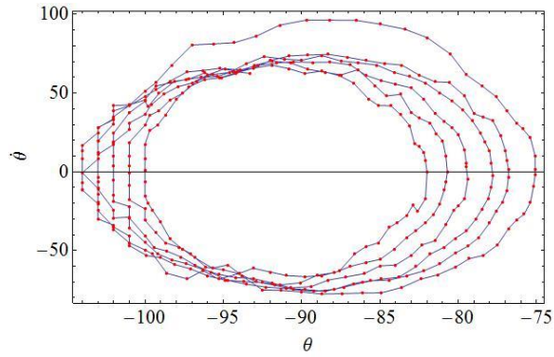

Graph 19 Trajectories corresponding to positions $(\theta, \dot{\theta})$ of the pendular mass m.

Following the pendular mass is complicated through *Tracker*, since the video only allows us to observe two dimensions. The results are affected both by the perspective, as well as the depth of the shot, also by the focus, so they contain a considerable experimental error. Graph 19 shows the phase plane of the variable θ, the curve is comparable to that shown in Graph 6 in two dimensions, showing a qualitative agreement between them.

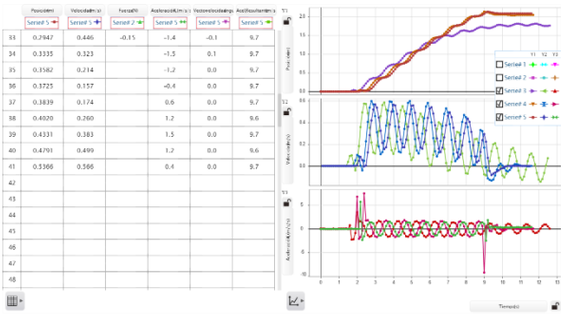

Graph 20 Results obtained by means of the sensor for linear motion

Graph 20 shows the results obtained by means of the sensor placed in the object of mass *M*. The first graph offers results for the position, observing the oscillations for three different experiments, these oscillations are also present in the graph corresponding to the simulation result. They differ in the trend of the slope. The second graph corresponds to that of the velocity in *y*, which is also comparable with the numerical result. The third graph is for acceleration, showing the same effect as in Graph 4, where some values are positive and negative.

UACM

The results corresponding to the circular motion are presented in Figure 7, where, again, the monitoring on the object of mass *M* moving on the rail forced to follow a circular motion is observed. The trajectory is drawn in red, while the monitoring of the pendular mass *m* is in blue, the monitoring of the rod is also shown.

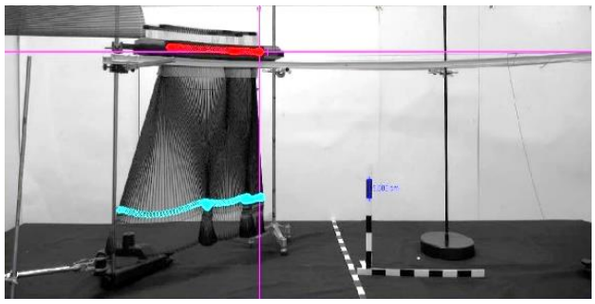

Figure 7 Trajectories corresponding to the positions of the pendular mass m and the object M in the circular motion

Figure 7 shows a qualitative agreement with the numerical result. To be clear on this, it is necessary to observe Graph 21, which shows the spiral behavior also shown by Graph 16.

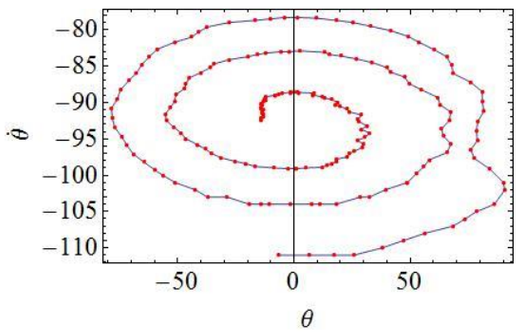

Graph 21 Results obtained by means of the sensor for linear motion

Finally, Graph 22 shows the results obtained by the sensor for the movement of the car of mass *M*.

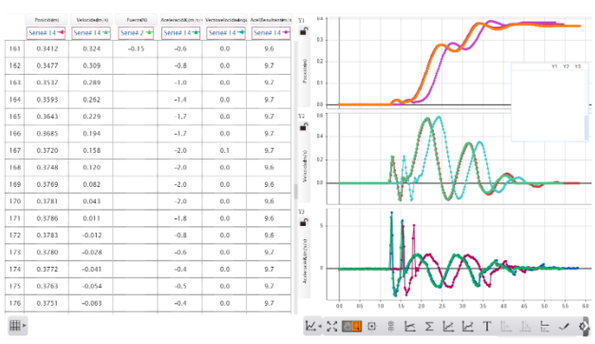

Graph 22 Results obtained by means of the sensor for circular motion

Conclusions

We have presented the theoretical analysis of the system composed of an object of mass *M* to which a pendulum of length *l* and pendular mass *m* was attached, moving in two kinds of movements: uniformly accelerated linear and uniformly accelerated circular motion. At first, we assumed that both movements were uniform; however, the analysis showed that due to the coupling of the objects and the oscillation of the pendulum the movement of the object of mass *M* was affected, so that its acceleration did not turn out to be uniform.

Theoretical analysis showed that despite being a system with variable acceleration, the linear momentum of the object of mass *M* was preserved, but not that of the pendular mass.

A set of numerical simulations was developed to obtain the solutions of the differential equations.

From the analysis of the numerical results, it is concluded that the system, both in linear and circular motion, is chaotic; thus, posing the possibility of studying them through the methodology used to analyze chaos, such as: Poincaré sections and Lyapunov coefficients, for example. In this way, it is possible to offer a more precise quantitative evaluation of the chaotic behavior of the system.

The corresponding experimental prototypes were developed to carry out a series of experiments and gather information with the use of proprietary tools such as *Tracker*. Likewise, wireless devices were used to phenomenologically verify both numerical and theoretical results. Because the experimental part requires even more care and that the pendulum movement occurs in 3D, a qualitative agreement was found in the comparisons made for the numerical and experimental results. However, we concluded that it is necessary to improve the obtention of the experimental results so that the comparison between the two is quantitative and not only qualitative.

The study of this kind of systems is important since they are commonly used, for example, in the handling of cranes that carry loads, airplanes and/or helicopters that carry buoys to put out fires.

The object transported behaves like the pendular mass and its oscillatory movement affects the movement of the transporting object. The analysis shown so far has allowed us to reach theoretical solutions, which enable us to understand the behavior of the system; along with numerical solutions that help to understand its tendency to chaos and also contribute to improve the use of its implementations; and experimental solutions that allow us to generate more adequate prototypes for the required purposes.

References.

Douglas Brown. (2013). Sharing video experiments with tracker digital libraries. May 15, 2019, from Tracker Website: https://physlets.org/tracker/

Enrique, C., Yanitelli, M., y Giorgi, S. (2019). Perfiles conceptuales como instrumentos de evaluación de una intervención didáctica. Avances en la enseñanza de la Física, 1(1), 73-99.

Herbert Goldstein, Charles Poole, John Safko. (2000). Classical Mechanics. New York: Addison Wesley.

Jaime De la Colina y Jesús Valdés. (2010). Péndulo de prueba para el estudio dinámico de modelos estructurales. Revista de Ingeniería Sísmica, No 82, pp 35-56. May 17, 2019, from Scielo Data base.

Jorge V. José and Eugene J. Saletan. (1998). Classical Dynamics. England: Cambridge University Press.

Lorena A. Lemus C. (2019). Simulación computacional, desarrollo teórico y comparación experimental de un péndulo elástico. Universidad de San Carlos de Guatemala Escuela de Ciencias Físicas y Matemáticas, Physics department: Bachelor thesis in Applied Physics.

Timothy Sauer. (2013). Numerical Methods. Chicago: PEARSON.

W. E. Boyce and R. C. Di Prima. (2004). Elementary Differential Equations and Boundary Value Problems. New York: Wiley.
Wolfram Research, Inc., Mathematica, Version 11.3, Champaign, IL (2018)

ISSN 2414-4924

Zúñiga, Francisco Agustín; Morales, Edgar Javier (2017). Diseño de una secuencia didáctica para el aprendizaje de la pendiente como razón de cambio para alumnos de nivel medio superior utilizando herramientas tecnológicas. In Serna, Luis Arturo (Ed.), Acta Latinoamericana de Matemática Educativa (pp. 1495-1504). Mexico, Mexico City: Comité Latinoamericano de Matemática Educativa.

ISSN 2414-4924

[Title in Times New Roman and Bold No. 14 in English and Spanish]

Surname (IN UPPERCASE), Name 1st Author†*, Surname (IN UPPERCASE), Name 1st Coauthor, Surname (IN UPPERCASE), Name 2nd Coauthor and Surname (IN UPPERCASE), Name 3rd Coauthor

Institutional Affiliation of Author including Dependency (No.10 Times New Roman and Italic)

International Identification of Science - Technology and Innovation

ID 1st Author: (ORC ID - Researcher ID Thomson, arXiv Author ID - PubMed Author ID - Open ID) and CVU 1st author: (Scholar-PNPC or SNI-CONACYT) (No.10 Times New Roman)

ID 1st Coauthor: (ORC ID - Researcher ID Thomson, arXiv Author ID - PubMed Author ID - Open ID) and CVU 1st coauthor: (Scholar or SNI) (No.10 Times New Roman)

ID 2nd Coauthor: (ORC ID - Researcher ID Thomson, arXiv Author ID - PubMed Author ID - Open ID) and CVU 2nd coauthor: (Scholar or SNI) (No.10 Times New Roman)

ID 3rd Coauthor: (ORC ID - Researcher ID Thomson, arXiv Author ID - PubMed Author ID - Open ID) and CVU 3rd coauthor: (Scholar or SNI) (No.10 Times New Roman)

(Report Submission Date: Month, Day, and Year); Accepted (Insert date of Acceptance: Use Only ECORFAN)

Abstract (In English, 150-200 words)

Objectives
Methodology
Contribution

Abstract (In Spanish, 150-200 words)

Objectives
Methodology
Contribution

Keywords (In English)

Indicate 3 keywords in Times New Roman and Bold No. 10

Keywords (In Spanish)

Indicate 3 keywords in Times New Roman and Bold No. 10

Citation: Surname (IN UPPERCASE), Name 1st Author, Surname (IN UPPERCASE), Name 1st Coauthor, Surname (IN UPPERCASE), Name 2nd Coauthor and Surname (IN UPPERCASE), Name 3rd Coauthor. Paper Title. ECORFAN Journal-Democratic Republic of Congo. Year 1-1: 1-11 [Times New Roman No.10]

* Correspondence to Author (example@example.org)
† Researcher contributing as first author.

Introduction

Text in Times New Roman No.12, single space.

General explanation of the subject and explain why it is important.

What is your added value with respect to other techniques?

Clearly focus each of its features

Clearly explain the problem to be solved and the central hypothesis.

Explanation of sections Article.

Development of headings and subheadings of the article with subsequent numbers

[Title No.12 in Times New Roman, single spaced and bold]

Products in development No.12 Times New Roman, single spaced.

Including graphs, figures and tables-Editable

In the article content any graphic, table and figure should be editable formats that can change size, type and number of letter, for the purposes of edition, these must be high quality, not pixelated and should be noticeable even reducing image scale.

[Indicating the title at the bottom with No.10 and Times New Roman Bold]

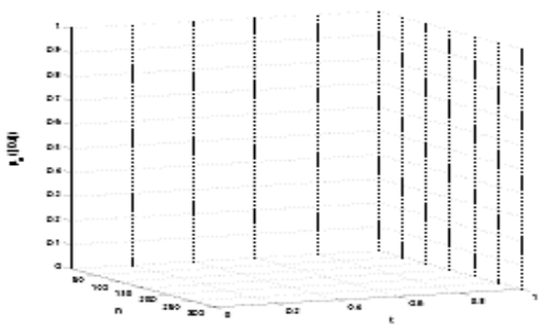

Graphic 1 Title and *Source (in italics)*

Should not be images-everything must be editable.

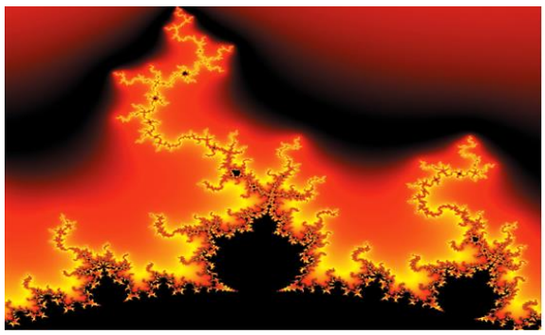

Figure 1 Title and *Source (in italics)*

Should not be images-everything must be editable.

Table 1 Title and *Source (in italics)*

Should not be images-everything must be editable.

Each article shall present separately in **3 folders**: a) Figures, b) Charts and c) Tables in .JPG format, indicating the number and sequential Bold Title.

For the use of equations, noted as follows:

$$Y_{ij} = \alpha + \sum_{h=1}^{r} \beta_h X_{hij} + u_j + e_{ij} \quad (1)$$

Must be editable and number aligned on the right side.

Methodology

Develop give the meaning of the variables in linear writing and important is the comparison of the used criteria.

Results

The results shall be by section of the article.

Annexes

Tables and adequate sources

Thanks

Indicate if they were financed by any institution, University or company.

Conclusions

Explain clearly the results and possibilities of improvement.

ISSN 2414-4924

References

Use APA system. Should not be numbered, nor with bullets, however if necessary numbering will be because reference or mention is made somewhere in the Article.

Use Roman Alphabet, all references you have used must be in the Roman Alphabet, even if you have quoted an Article, book in any of the official languages of the United Nations (English, French, German, Chinese, Russian, Portuguese, Italian, Spanish, Arabic), you must write the reference in Roman script and not in any of the official languages.

Technical Specifications

Each article must submit your dates into a Word document (.docx):

Journal Name
Article title
Abstract
Keywords
Article sections, for example:

1. *Introduction*
2. *Description of the method*
3. *Analysis from the regression demand curve*
4. *Results*
5. *Thanks*
6. *Conclusions*
7. *References*

Author Name (s)
Email Correspondence to Author
References

Intellectual Property Requirements for editing:

-Authentic Signature in Color of Originality Format Author and Coauthors

-Authentic Signature in Color of the Acceptance Format of Author and Coauthors

ISSN 2414-4924

Reservation to Editorial Policy

ECORFAN-Democratic Republic of Congo reserves the right to make editorial changes required to adapt the Articles to the Editorial Policy of the Journal. Once the Article is accepted in its final version, the Journal will send the author the proofs for review. ECORFAN® will only accept the correction of errata and errors or omissions arising from the editing process of the Journal, reserving in full the copyrights and content dissemination. No deletions, substitutions or additions that alter the formation of the Article will be accepted.

Code of Ethics - Good Practices and Declaration of Solution to Editorial Conflicts

Declaration of Originality and unpublished character of the Article, of Authors, on the obtaining of data and interpretation of results, Acknowledgments, Conflict of interests, Assignment of rights and Distribution

The ECORFAN-Mexico, S.C Management claims to Authors of Articles that its content must be original, unpublished and of Scientific, Technological and Innovation content to be submitted for evaluation.

The Authors signing the Article must be the same that have contributed to its conception, realization and development, as well as obtaining the data, interpreting the results, drafting and reviewing it. The Corresponding Author of the proposed Article will request the form that follows.

Article title:

– The sending of an Article to ECORFAN-Democratic Republic of Congo emanates the commitment of the author not to submit it simultaneously to the consideration of other series publications for it must complement the Format of Originality for its Article, unless it is rejected by the Arbitration Committee, it may be withdrawn.

– None of the data presented in this article has been plagiarized or invented. The original data are clearly distinguished from those already published. And it is known of the test in PLAGSCAN if a level of plagiarism is detected Positive will not proceed to arbitrate.

– References are cited on which the information contained in the Article is based, as well as theories and data from other previously published Articles.

– The authors sign the Format of Authorization for their Article to be disseminated by means that ECORFAN-Mexico, S.C. In its Holding Democratic Republic of Congo considers pertinent for disclosure and diffusion of its Article its Rights of Work.

– Consent has been obtained from those who have contributed unpublished data obtained through verbal or written communication, and such communication and Authorship are adequately identified.

– The Author and Co-Authors who sign this work have participated in its planning, design and execution, as well as in the interpretation of the results. They also critically reviewed the paper, approved its final version and agreed with its publication.

– No signature responsible for the work has been omitted and the criteria of Scientific Authorization are satisfied.

– The results of this Article have been interpreted objectively. Any results contrary to the point of view of those who sign are exposed and discussed in the Article.

Copyright and Access

The publication of this Article supposes the transfer of the copyright to ECORFAN-Mexico, SC in its Holding Democratic Republic of Congo for its ECORFAN-Democratic Republic of Congo, which reserves the right to distribute on the Web the published version of the Article and the making available of the Article in This format supposes for its Authors the fulfilment of what is established in the Law of Science and Technology of the United Mexican States, regarding the obligation to allow access to the results of Scientific Research.

Article Title:

Name and Surnames of the Contact Author and the Coauthors	Signature
1.	
2.	
3.	
4.	

Principles of Ethics and Declaration of Solution to Editorial Conflicts

Editor Responsibilities

The Publisher undertakes to guarantee the confidentiality of the evaluation process, it may not disclose to the Arbitrators the identity of the Authors, nor may it reveal the identity of the Arbitrators at any time.

The Editor assumes the responsibility to properly inform the Author of the stage of the editorial process in which the text is sent, as well as the resolutions of Double-Blind Review.

The Editor should evaluate manuscripts and their intellectual content without distinction of race, gender, sexual orientation, religious beliefs, ethnicity, nationality, or the political philosophy of the Authors.

The Editor and his editing team of ECORFAN® Holdings will not disclose any information about Articles submitted to anyone other than the corresponding Author.

The Editor should make fair and impartial decisions and ensure a fair Double-Blind Review.

Responsibilities of the Editorial Board

The description of the peer review processes is made known by the Editorial Board in order that the Authors know what the evaluation criteria are and will always be willing to justify any controversy in the evaluation process. In case of Plagiarism Detection to the Article the Committee notifies the Authors for Violation to the Right of Scientific, Technological and Innovation Authorization.

Responsibilities of the Arbitration Committee

The Arbitrators undertake to notify about any unethical conduct by the Authors and to indicate all the information that may be reason to reject the publication of the Articles. In addition, they must undertake to keep confidential information related to the Articles they evaluate.

Any manuscript received for your arbitration must be treated as confidential, should not be displayed or discussed with other experts, except with the permission of the Editor.

The Arbitrators must be conducted objectively, any personal criticism of the Author is inappropriate.

The Arbitrators must express their points of view with clarity and with valid arguments that contribute to the Scientific, Technological and Innovation of the Author.

The Arbitrators should not evaluate manuscripts in which they have conflicts of interest and have been notified to the Editor before submitting the Article for Double-Blind Review.

Responsibilities of the Authors

Authors must guarantee that their articles are the product of their original work and that the data has been obtained ethically.

Authors must ensure that they have not been previously published or that they are not considered in another serial publication.

Authors must strictly follow the rules for the publication of Defined Articles by the Editorial Board.

The authors have requested that the text in all its forms be an unethical editorial behavior and is unacceptable, consequently, any manuscript that incurs in plagiarism is eliminated and not considered for publication.

Authors should cite publications that have been influential in the nature of the Article submitted to arbitration.

Information services

Indexation - Bases and Repositories

RESEARCH GATE (Germany)
GOOGLE SCHOLAR (Citation indices-Google)
REDIB (Ibero-American Network of Innovation and Scientific Knowledge- CSIC)
MENDELEY (Bibliographic References Manager)

Publishing Services

Citation and Index Identification H
Management of Originality Format and Authorization
Testing Article with PLAGSCAN
Article Evaluation
Certificate of Double-Blind Review
Article Edition
Web layout
Indexing and Repository
ArticleTranslation
Article Publication
Certificate of Article
Service Billing

Editorial Policy and Management

31 Kinshasa 6593 – Republique Démocratique du Congo. Phones: +52 1 55 6159 2296, +52 1 55 1260 0355, +52 1 55 6034 9181; Email: contact@ecorfan.org www.ecorfan.org

ECORFAN Journal-Democratic Republic of Congo

2414 4924
ISSN 2414 - 4924

www.ecorfan.org